almost symmetrically, with Cu-N distances of 1.969(1) and 1.994(1) Å, and a bite angle of 92.0 (6)°. The equatorial Cu(1)-O(1) and Cu(1)-O(4) bond distances are slightly shorter with values of 1.946(1) and 1.919(1) Å. The third oxygen atom from hydrogenphosphate group is bent towards the Cu atom to complete a fifth coordination site in an axial position at a much longer distance of 2.719(2) Å, generating a distorted square-based pyramidal stereochemistry. The four in-plane atoms, N(1), N(2), O(1) and O(4) are not planar (r.m.s. deviation 0.562 Å) and display a marked tetrahedral twist (dihedral angles between the CuN_2 and CuO_2 planes amounts to 45.56°). The Cu atom lies 0.202 Å above this plane towards O(2A). The copper chromophore can be described as having an extremely tetrahedrally distorted square pyramidal geometry with the tetragonality, T of 0.720 and τ-value of 0.12. The Cu-Cu distance is 5.955(2) Å.

The hydrogenphosphato group in this compound involves a quite unusual tridentate μ_2,η^3 coordination mode: didentately coordinated to one copper chromophore and monodentately bonded to another. To the best of our knowledge this coordination mode of the bridging hydrogenphosphate present in complex **II** is unique for the transition metal complexes.

The coordinated P=O bonds, 1.519(1), 1.510(2) and 1.531(1) Å, are shorter than the uncoordinated P-OH bond, 1.588(2) Å. This is usually found for the three-coordinate bridging coordination of the hydrogenphosphate anion. The tridentate hydrogenphosphato group involves O-P-O angles ranging from 101.9(1) to 111.7(1)°. The lattice structure is stabilized by a hydrogen-bonding network between the amine N and an oxygen atom of the hydrogenphosphate group with a short contact distance of 2.663(3) Å and between the oxygen atom of the hydrogenphosphate group to the oxygen atom of another phosphatogroup with a contact distance of 2.528(3) Å. The structure contains chains of Cu ions in the c-direction bridged by the HPO_4^{2-} ions in a trigonal way. Two nearest Cu(II) ions are bridged by a tridentate hydrogenphosphate group which is didentately coordinated to one copper(II) ion, and monodentately coordinated to another in an equatorial-equatorial configuration in an unusual bridging coordination mode. The helical arrangement of the Cu-HPO_4 chain is clearly visible in Fig. 3 with the N ligands at the outside stacked in the direction of the 3-fold screw axis.

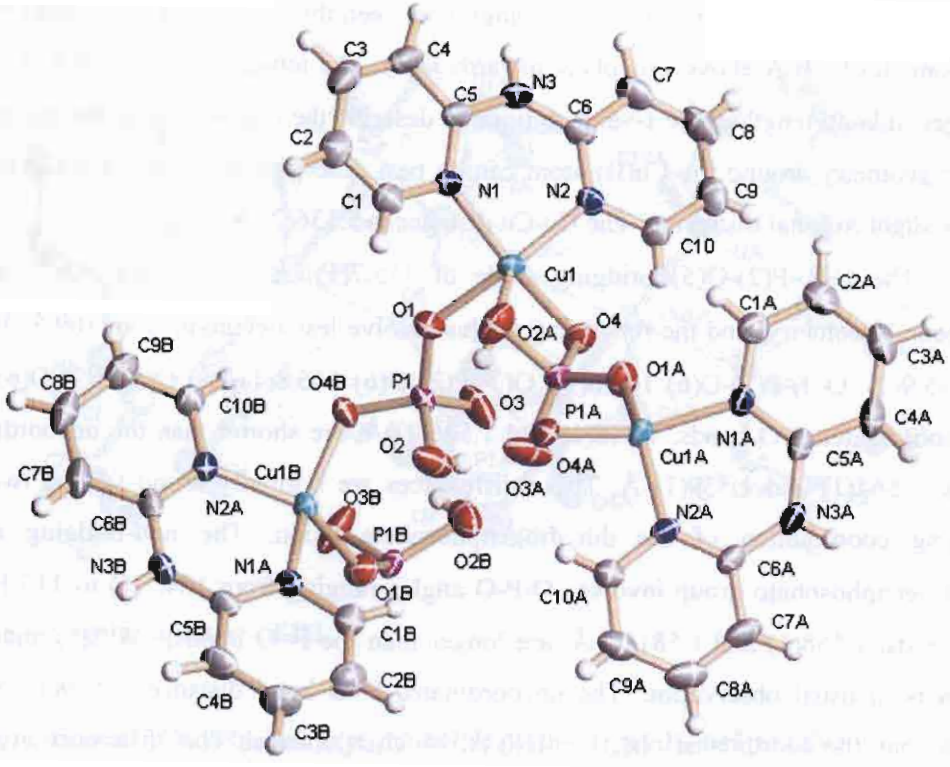

Figure 3 The polymeric structure of **II**

2.4.1.3 Description of $[Cu(dpyam)(\mu_2, \eta^2\text{-}H_2PO_4)(H_2PO_4)]_2$ (III)

The structure is depicted in Fig. 4 together with the numbering scheme. Selected bond distances and angles are listed in Table 4, Appendix IIB. The centrosymmetric dinuclear compound consists of two $[Cu(dpyam)(\mu_2,\eta^2\text{-}H_2PO_4)(H_2PO_4)]$ units being doubly bridged by two didentate dihydrogenphosphato anions. The local molecular structure of the copper atom involves a square pyramidal CuN_2O_2O' chromophore. The basal plane consists of two oxygen atoms of the two bridging dihydrogenphosphato groups, O(5) and O(8A) and of dpyam ligand coordinated through two nitrogen atoms. The dpyam ligand chelates in the square plane, almost symmetrically, with Cu-N distances of 1.991(1) and 1.997(1) Å and a bite angle of 88.1(1)°. The equatorial Cu(1)-O(8A) and Cu(1)-O(5) bond distances are slightly shorter with values of 1.964 (1) and 1.987(1) Å. The fifth axial coordination site is occupied by one oxygen atom of non-bridging monodentate dihydrogenphosphato group at the Cu-O distance of 2.271(1) Å. The four in-plane atoms, N(1), N(2), O(5) and O(8A) are essentially planar, (r.m.s. deviation 0.0598 Å)

with a slightly tetrahedral twist (dihedral angles between the CuN_2 and CuO_2 planes = 14.0°). The Cu atom lies 0.16 Å above this plane towards O(1). The tetragonality, T = 0.874 based on the changes in bond lengths. The τ-value defined to describe the degree of trigonal distortion is 0.12, so the geometry around the Cu(II) atom can be best described as square-based pyramidal, with only a slight trigonal distortion. The Cu-Cu distance is 5.136(2) Å.

The O(8)-P(2)-O(5) bridging angle of 115.7(1)° is larger than 109.5° of the ideal tetrahedral geometry, and the remaining angles involve less deviation from 109.5° [O(5)-P(2)-O (7) 105.9(1), O(5)-P(2)-O(6) 105.6(1), O(7)-P(2)-O(6) 106.8(1) and O(8)-P(2)-O(6) 112.6(1)°]. The coordinated P-O bonds, 1.518(1) and 1.506(1) Å, are shorter than the uncoordinated P-OH bonds, 1.564(1) and 1.559(1) Å. These differences are normally found for the two-coordinate bridging coordination of the dihydrogenphosphate anion. The non-bridging monodentate dihydrogenphosphato group involves O-P-O angles ranging from 104.1(1) to 115.1(1)°. The P-OH bonds, 1.558(1) and 1.581(1) Å, are longer than the P=O bonds, 1.512(1) and 1.519(1) Å, which is in usual observation. The uncoordinated P=O bond distance, 1.519(1) Å, is slightly longer than the coordinated one, 1.511(1) Å, which is unusual. This difference arises from the hydrogen bond involved to the uncoordinated P=O bond. The P=O distances in both the monodentate dihydrogenphosphato group and the dihydrogenphosphato bridge are ranging from 1.506(1) to 1.519(1) Å, while the P-OH bond distances vary from 1.558(1) to 1.581(1) Å. This behavior is consistent with the general observation that P-OH bonds are longer than P=O bonds in primary and secondary phosphates.

The lattice structures are stabilized by a hydrogen bonding network between the amine N and the oxygen atom of the non-bridged dihydrogenphosphate anion with a distance of 3.1603 (19) Å, and between oxygen atoms of different dihydrogenphosphate groups (O···O distances vary from 2.5825(18) to 2.648(2) Å).

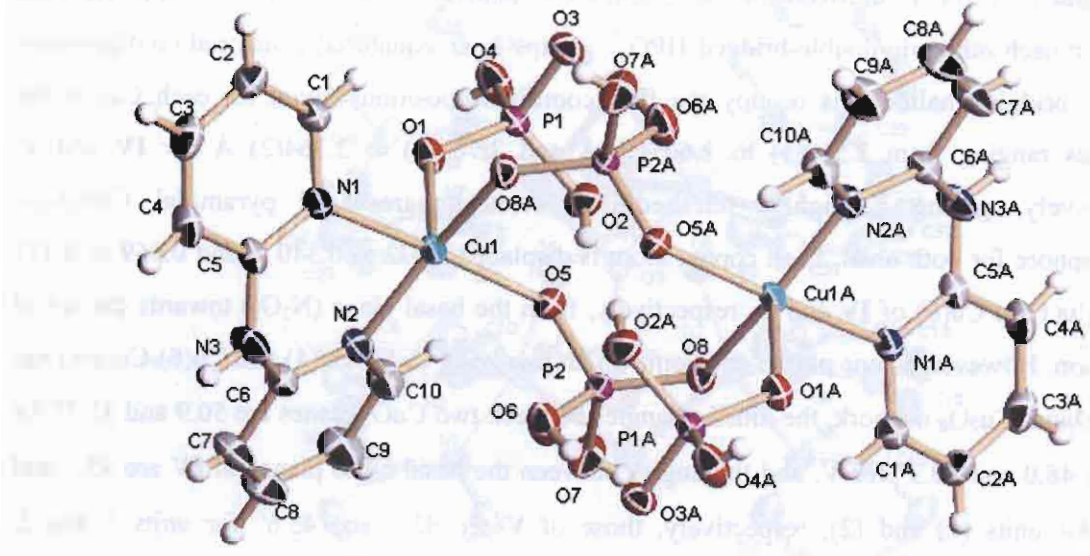

Figure 4 The molecular structure of **III**

2.4.1.4 Description of $[Cu_4(dpyam)_4(\mu_4,\eta^3\text{-}HPO_4)_2(\mu\text{-}Cl)_2](Cl)_2{\cdot}6H_2O$ (IV) and $[Cu_4(dpyam)_4(\mu_4,\eta^3\text{-}HPO_4)_2(\mu\text{-}Br)_2](Br)_2{\cdot}6H_2O$ (V)

The structure of **IV** consists of two independent tetranuclear units of $[Cu_4(dpyam)_4(\mu_4,\eta^3\text{-}HPO_4)_2(\mu\text{-}Cl_2)]^{2+}$, namely units (1) and (2), four chloride anions and twelve lattice water molecules. Unit (1) is situated in a general position, whereas unit (2) is situated on a mirror plane. The unit cell contains four molecules on general positions and two molecules on special positions. Compound **V** is isostructural and involves similar asymmetric unit and similar structure to those of **IV.** An ORTEP plot, together with the numbering scheme of the compounds are shown in Figs. 5 and 6, with relevant distances and angles in Tables 5 and 6, Appendix IIB.

The tetranuclear unit of both compounds consists of two pairs of five coordinated copper (II) ions bridged by two tetrahedral tridentate hydrogenphosphato groups in each molecule. Both HPO_4^{2-} groups coordinate monodentately to each copper(II) ion and bridging via one oxygen to two other Cu(II) ions, giving a μ_4,η^3 coordination mode which is rarely found in the hydrogenphosphate metals. Each copper ion involves an essentially planar square base of the CuN_2O_2X chromophore through the two bridging HPO_4^{2-} groups and a terminal dpyam ligand with a slight tetrahedral twist (evident from the dihedral angles of 18.06,19.38, 5.68, 6.66,23.59 and 6.20° for Cu(1) to Cu(6) chromophores, respectively, for **IV** and 17.63, 19.21, 4.53, 5.40,

22.25 and 5.11° for **V**, between the CuO_2 and CuN_2 planes). Consequently, all copper(II) ions linked to each other via double-bridged HPO_4^{2-} groups in an equatorial-equatorial configuration. Finally, bridging halide ions occupy the fifth coordinate positions (axial for each Cu) at the distances ranging from 2.559(1) to 2.603(1) Å and 2.707(2) to 2.764(2) Å for **IV** and **V**, respectively, giving a slightly tetrahedral-distorted square-based pyramidal CuN_2O_2X chromophore for both units. Each copper atom is displaced 0.072 to 0.340 Å and 0.069 to 0.337 Å for Cu(1) to Cu(6) of **IV** and **V**, respectively, from the basal plane (N_2O_2) towards the apical halide ion. However, as one pair of each unit which involving Cu(3)-Cu(4) and Cu(6)-Cu(6A) has a non-planar Cu_2O_2 network, the dihedral angles between two CuO_2 planes are 50.9 and 51.7° for **IV** and 48.0 and 50.3° for **V**, and the angles between the basal N_2O_2 planes of **IV** are 45.1 and 45.9° for units (1) and (2), respectively, those of **V** are 43.3 and 45.6° for units 1 and 2, respectively, indicating a roof-shaped structure. The τ values vary from 0.020 to 0.053 and 0.001 to 0.071 for **IV** and **V**, respectively, indicating the nearly perfect square-based pyramidal geometry for all CuN_2O_2X chromophores. The Cu...Cu distances in **IV** are ranging from 2.802(1) Å, in the dinuclear units to 5.224(1) Å in the tetranuclear units and those of **V** are ranging from 2.834(1) to 5.2339(1) Å.

The P-OH bonds which are ranging from 1.533(10) to 1.629(10) Å for **V**, are longer than the P-O bonds (1.475(8)-1.599(10) Å **V**), which are in usual observation except those of P(1)-O (3) (1.599(10)Å), P(2)-O(7) (1.589(9)Å), and P(4)-O(12) (1.555(11)Å) in **V**. This arises may be due to the hydrogen bonding between these oxygen atoms and the hydrogen atoms attached to carbon atom from the amine groups. These hydrogen bonds may be co-responsible for the evident longer P-O bonds.

The lattice structure is stabilized by a hydrogen-bonding network (D...A distances) N-H...X(uncoor., 3.246-3.419 Å for **IV** and 3.369-3.542 Å for **V**), O(HPO_4)-H...O(W) (2.590-2.638 Å for **IV** and 2.588-2.700 Å for **V**), and O(W)-H...Br(uncoor., 3.144-3.274 for **IV** and 3.276-3.669 Å for **V**) and O(W)-H...O(W) (2.664 Å for **IV** and 2.664-3.738 Å for **V**).

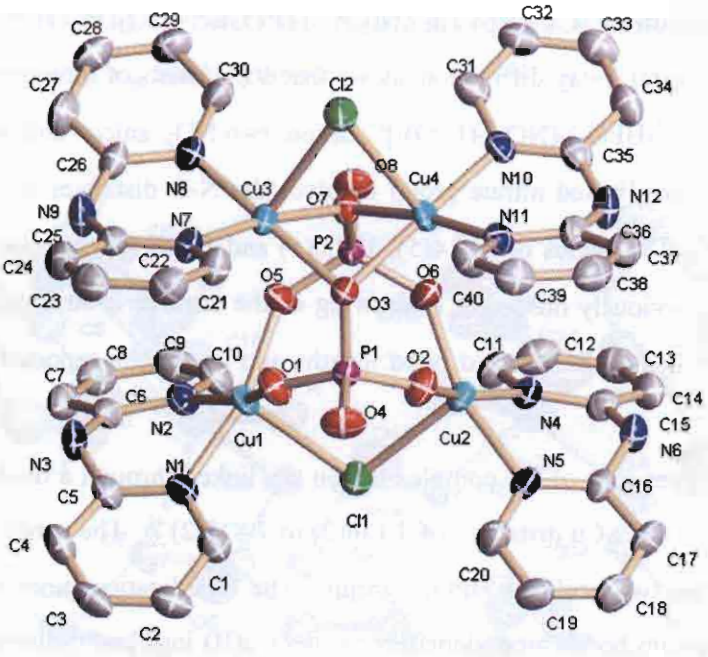

Figure 5 The molecular structure of **IV**

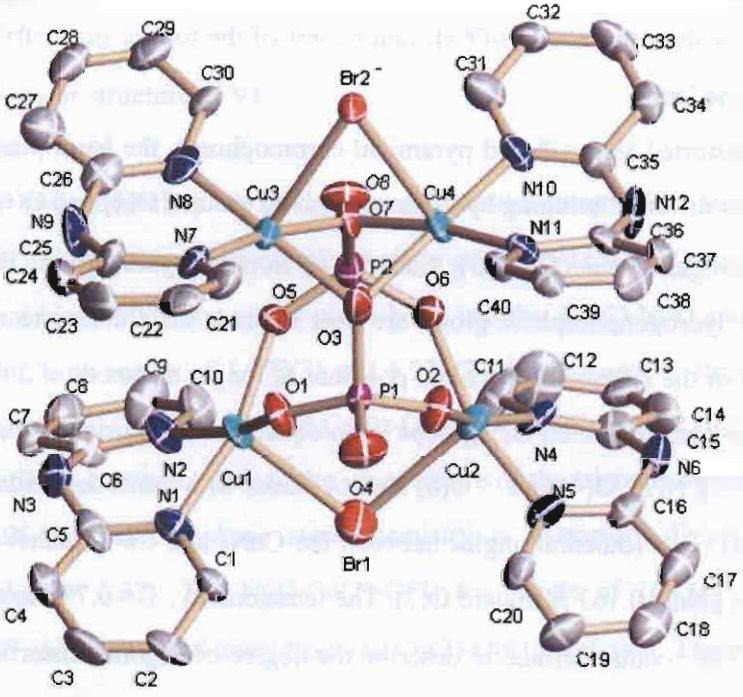

Figure 6 The molecular structure of **V**

2.4.1.5 Description of $[Cu_4(dpyam)_4(\mu_3,\eta^3\text{-}HPO_4)_2(NO_3)_2(H_2O)_2](NO_3)_2 \cdot 2H_2O$ (VI)

Single crystal X-ray diffraction shows that **VI** consists of a centrosymmetric tetranuclear $[Cu_4(dpyam)_4(\mu_3,\eta^3\text{-}HPO_4)_2(NO_3)_2(H_2O)_2]^{2+}$ cation, two NO_3^- anions and two molecules of lattice water. The non-coordinated nitrate group involves the N-O distances of 1.233(5), 1.236(6) and 1.23(5) Å and O-N-O angles of 119.4(5), 120.0(5) and 120.6(5)°, in good agreement with those of the free ion previously observed. A drawing of the tetrameric structure showing the labeling scheme is given in Fig. 7. Selected bond lengths and angles are reported in Table 7, Appendix IIB.

Four copper ions of the complex cation are linked through a double hydrogenphosphate bridge, leading to Cu...Cu distances of 4.136(2) to 7.833(2) Å. The cation is located on a c glide plane through the two bridging HPO_4^{2-} groups. The coordination mode of HPO_4^{2-} is tridentate bridging, each group bonds monodentately to two Cu(II) ions and didentately coordinated to the third one giving a novel μ_3,η^3 coordination mode. Compound **VI** has mixed stereochemistries of a tetrahedral distorted square-based pyramid (τ = 0.32) and an intermediate geometry between regular trigonal bipyramid and regular square pyramid (τ = 0.52) within a tetranuclear unit. The tetranuclear unit involves two CuN_2O_2O' chromophores of the former geometry and two CuN_2O_3 chromophores of the latter.

For two distorted square-based pyramidal chromophores, the basal plane consists of two oxygen atoms from different bridging hydrogenphosphato groups, O(4) and O(6) (1.968(2), 1.972 (2) Å) and two nitrogen atoms (1.967(3), 2.001(3) Å) from a dpyam ligand. The second oxygen atoms from each hydrogenphosphate group are bent towards the Cu ions to complete the fifth coordination sites in the approximately axial positions at longer distances of 2.497(2) Å. Two Cu ions are doubly bridged by the HPO_4^{2-} groups in an equatorial-equatorial configuration. The four in-plane atoms, N(1), N(2), O(4) and O(6) are not planar with r.m.s. deviation of 0.473 Å and a marked tetrahedral twist (dihedral angles between the CuN_2 and CuO_2 planes = 41.2°). The Cu ion lies above this plane, 0.163 Å toward O(7). The tetragonality, T = 0.791 based on the changes in bond lengths. The τ-value defined to describe the degree of trigonal distortion is 0.32. As the regular trigonal bipyramid and square-based pyramid have τ values of 1.00 and 0.00, respectively, the stereochemistry of the CuN_2O_2O' chromophore of **VI** is best described as

extremely tetrahedral-distorted square-based pyramidal with a slight trigonal distortion, rather than square pyramidal distorted trigonal bipyramidal.

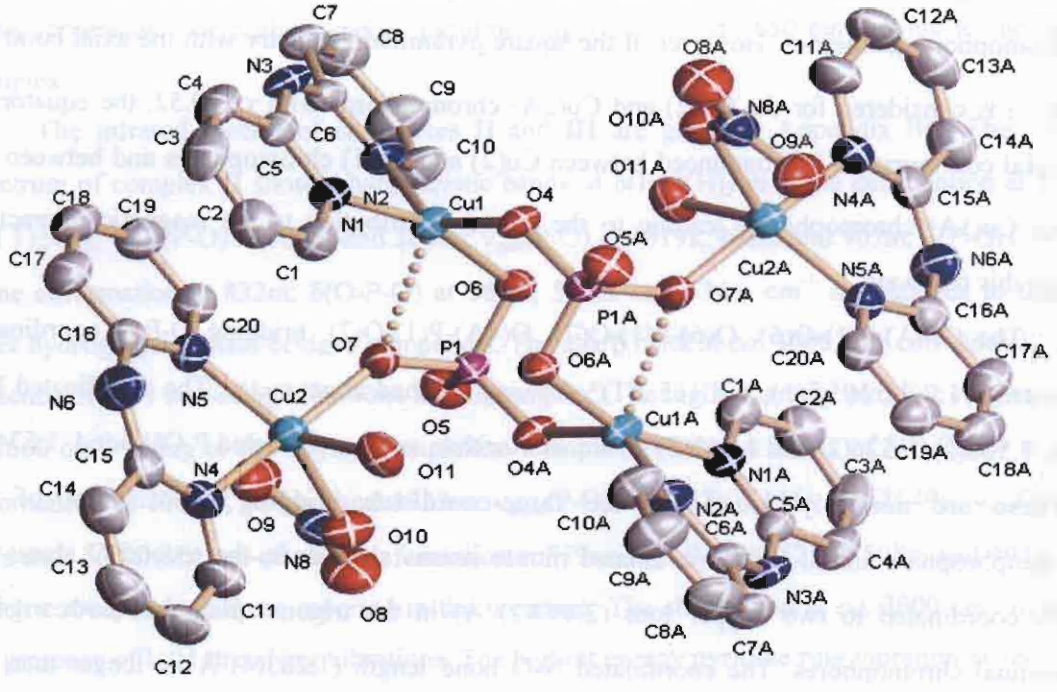

Figure 7 The molecular structure of **VI**

The other two equivalent chromophores within the tetranuclear unit involve a five coordinate CuN_2O_3 chromophore, with an intermediate geometry ($\tau = 0.52$) but slightly distorted towards the trigonal bipyramid. The out-of-plane bond lengths, Cu(2)-N(4) and Cu(2)-O(7), are significantly shorter, with values of 1.979(3) and 1.933(2) Å, compared to those of the in-plane bond lengths, Cu(2)-N(5), Cu(2)-O(10) and Cu(2)-O(11), with values of 2.013(3), 2.145(3) and 2.152(3) Å, respectively, corresponding to the usual nature of the trigonal bipyramidal geometry. However, the CuN_2O_2O' chromophore stereochemistry is extremely distorted from regular trigonal pyramidal ($\tau = 0.52$). The N(4)-Cu(2)-O(7) (α_8) angle of 168.6(1)° is significantly different from 180° and is distorted away from the Cu(2)-O(11) direction. The in-plane angles, N(5)-Cu(2)-O(11) (α_1), N(5)-Cu(2)-O(10) (α_2) and O(10)-Cu(2)-O(11) (α_3), are all significantly different from 120°, namely 131.1(1), 137.5(1) and 91.2(1)°, respectively. A pair of the extremely

distorted trigonal bipyramidal Cu(2) and Cu(2A) chromophores is non-bridged, but each chromophore is linked to the distorted square pyramidal Cu(1) and Cu(1A) chromophores via a HPO_4^{2-} group in an axial-equatorial configuration. Additionally, the axial-axial configuration (pathways Cu(1)-O(7)-Cu(2) and Cu(1A)-O(7A)-Cu(2A)) is also exist between these two types of the chromophore geometries. However, if the square pyramidal geometry with the axial bond Cu (2)-O(11) is considered for the Cu(2) and Cu(2A) chromophores with $\tau = 0.52$, the equatorial-equatorial configuration is pronounced between Cu(2) and Cu(1) chromophores and between Cu (2) and Cu(1A) chromophores, leading to the partial contribution to the magnetic interaction through this pathway.

The O(4A)-P(1)-O(6), O(6)-P(1)-O(7), O(4A)-P(1)-O(7), bridging O-P-O coordinated angles are 111.7(1), 105.3(1), and 115.2(1)° showing tetrahedral geometry. The coordinated P-O bonds, 1.526(2), 1.526(2) and 1.542(2) Å, are shorter than an uncoordinated P-OH bond, 1.574(2) Å. These are normally found for the three-coordinate bridging coordination of the hydrogenphosphate anion. Both coordinated nitrate anions are planar, the second O atoms are weakly coordinated to two copper ions (2.497(2) Å) in the trigonal planes of both trigonal bipyramidal chromophores. The coordinated N-O bond length (1.283(4) Å) is longer than the uncoordinated N-O bonds (1.233(4) and 1.249(4) Å) as well as the larger O-N-O angles of 122.2(3) and 119.5(3)° compared to the uncoordinated O-N-O one (118.3(3)°), corresponding to the typical feature of the monodentate nitrite group.

The lattice structure is stabilized by the hydrogen-bonding network N-H...O(HPO_4), O (HPO_4)-H...O($W_{uncoor.}$) and O($W_{coor.}$)-H...O(HPO_4) and O($W_{coor.}$)-H...O($W_{uncoor.}$).

2.4.2 IR spectra

The infrared spectrum of **I** (as in Appendix IIC) displays the characteristic bands of the hydrogenphosphate bridging ligand: δ(P-O(H)) in-plane deformation at 1240m and 1164m; ν_{asym} (P-O) at 1110s, 1071s and 1056m; ν_{sym}(P-O) at 1015s and 984m; δ(P-O(H)) out-of-plane deformation at 883m; δ(O-P-O) at 558m and 499m cm^{-1} corresponds to those of other hydrogenphosphato-bridged copper(II) complexes. This indicates that the hydrogenphosphate and phosphate ions are present as a bridging of mixed hydrogenphosphate and phosphate ligands. The

PF_6^- group vibration near 900 cm^{-1} splitting into a sharp peak at *ca.* 842 cm^{-1} indicates the PF_6^- ions in **I**. The sharp band at *ca.* 3000 cm^{-1} was observed, indicative of the presence of N-H stretching vibrations in this complex. The occurrence of a strong and broad absorption centered at 3419 cm^{-1} (symmetric and antisymmetric OH stretchings) is consistent with the crystallization water molecules. The highest energy pyridine ring vibration at 1650 cm^{-1} owing to the dpyam complex.

The infrared spectra of complexes **II** and **III** are given in Appendix IIC. The infrared spectrum of complex **II** shows characteristic bands of δ(P-O(H)) in-plane deformation at 1238m and 1156m; ν_{asym}(P-O) at 1092s and 1056s; ν_{sym}(P-O) at 1019s, 968m and 907m; δ(P-OH) out-of-plane deformation at 832m; δ(O-P-O) at 586m, 555m and 534m cm^{-1} corresponds to those of other hydrogenphosphato-bridged complexes. The sharp band at *ca.* 3000 cm^{-1} corresponds to the presence of N-H stretching vibrations in this complex. The highest energy pyridine ring vibration at 1660 cm^{-1} owing to the dpyam complexes. Complex **III** shows bands of δ(P-O(H)) in-plane deformation at 1354w, 1274m and 1232m; ν_{asym}(P-O) at 1157s, 1116s and 1049s; ν_{sym}(P-O) at 977s and; δ(P-O(H)) out-of-plane deformation at 879m; δ(O-P-O) at 525m, 508m and 491m cm^{-1} which corresponds to those reported in the literature. The sharp band at *ca.* 3000 cm^{-1} indicates the presence of N-H stretching vibrations. The highest energy pyridine ring vibration at 1633 cm^{-1} owing to the dpyam complexes.

The infrared spectrum of **IV** (as in Appendix IIC) displays the characteristic bands of the hydrogenphosphate bridging ligand: δ(P-O(H)) in-plane deformation at 1349m and 1235m; ν_{asym} (P-O) at 1159s, 1096s and 1054s; ν_{sym}(P-O) at 1019m, 976m and 936m; δ(O-P-O) at 529m and 511m cm^{-1} corresponds to those of other hydrogenphosphato-bridged copper(II) complexes, Table 2.2. The sharp band at *ca.* 3000 cm^{-1} was observed, indicative of the presence of N-H stretching vibrations in this complex. The crystallisation water molecules are consistent with the occurrence of a strong and broad absorption centered at 3422 cm^{-1} (symmetric and asymmetric OH stretchings). The highest energy pyridine ring vibration at 1630 cm^{-1} owing to the dpyam complexes.

The infrared spectra of complexes **V** and **VI** are given in Appendix IIC. Complex **V** shows characteristic bands of δ(P-O(H)) in-plane deformation at 1354m and 1236m; ν_{asym}(P-O) at 1159s, 1098m and 1054m; ν_{sym}(P-O) at 1019m, 980m and 938m; δ(O-P-O) at 529m and 511m cm^{-1} corresponds to those of other hydrogenphosphato-bridged copper(II) complexes. That of **VI**

shows band of δ(P-O(H)) in-plane deformation at 1238m; ν_{asym}(P-O) at 1156w, 1110s and 1056s; ν_{sym}(P-O) at 1012m; δ(P-O(H)) out-of plane deformation at 842m and δ(O-P-O) at 530w and 506w cm^{-1} corresponds to those of hydrogenphosphate anions and ν_{asym}(N-O) at 1384s and ν_{sym} (N-O) at 1312m cm^{-1} attributed to the coordinated nitrate group. The sharp band at *ca.* 3000 cm^{-1} for **V** and **VI** indicates of the presence of N-H stretching vibrations in these complexes. The occurrence of a strong and broad absorption centered at 3412 cm^{-1} for **V** and at 3429 cm^{-1} for **VI** (symmetric and asymmetric OH stretchings) are consistent with the presence of crystallization water molecules in both complexes. The highest energy pyridine ring vibration at 1633 cm^{-1} for **V** and at 1643 cm^{-1} for **VI** is owing to the dpyam complexes.

2.4.3 Electronic Reflectance spectra

The electronic diffuse reflectance spectrum of **I** (Fig. 8) shows a broad band ranging from 10.02 to 15.60 kK (centred at ca. 12.46 kK) where kK = 1000 cm^{-1}. This observed single broad peak is consistent with the mixed stereochemistries: the distorted square pyramidal geometry (τ = 0.17 and 0.13) which results in a typical main peak around 14.00-15.00 kK and a shoulder around 11.00-12.00 kK, usually observed for the regular square pyramidal geometry and the intermediate five-coordinate geometry (τ = 0.57) which displays a typical single broad peak around 12.00-13.00 kK, usually observed for the intermediate five-coordinated geometry. If the distorted trigonal bipyramidal geometry is considered for the intermediate five-coordinate geometry, a single broad peak appeared at the lower frequency side of a broad band may be assigned as the d_{xy}, d_{xz}, d_{yz}, $d_{x^2-y^2} \rightarrow d_{z^2}$ transition. In addition, that of the distorted square pyramidal geometry which appeared at the higher frequency side of a broad band may be assigned as the d_{z^2}, d_{xy}, d_{xz}, $d_{yz} \rightarrow d_{x^2-y^2}$ transition. However, there is a comparable feature with the electronic spectra of **II** and **III** (Fig. 8), in that **II** also exhibits a main peak at 14.44 kK with a shoulder at 11.20 kK. This observation corresponds to the d_{xy}, $d_{z^2} \rightarrow d_{x^2-y^2}$ transition for the low-energy peak and the d_{xz}, $d_{yz} \rightarrow d_{x^2-y^2}$ transition for the high-energy peak of the distorted square pyramidal geometry usually observed. Complex **III** displays a broad band at ca. 14.88 kK. This observed single broad peak is consistent with the square pyramidal stereochemistry and assigned to be d_{z^2}, d_{xy}, d_{xz}, $d_{yz} \rightarrow d_{x^2-y^2}$ transition.

The electronic diffuse reflectance spectrum of **IV** consists of an unsymmetrical, broad band centered at ca. 14.97 kK (Fig. 9) which is very comparable to that of **V** (14.88 kK) (Fig. 9). This

observed single broad peak is consistent with the square pyramidal stereochemistry and assigned to be the d_{z2}, d_{xy}, d_{xz}, $d_{yz} \rightarrow d_{x2-y2}$ transition. However, there is a comparable feature in electronic spectrum of **VI** (Fig. 9), which also shows a broad band ranging from 11.40 to 13.90 kK (centered at ca. 12.32 kK). The observed single broad peak in **VI** is consistent with the mixed stereochemistries: the distorted square pyramidal geometry (τ = 0.32) with a remarkable tetrahedral twist of the square base which results in the lower frequency of the spectrum as compared to that of the regular square pyramidal geometry (ca. 14.00-15.50 kK) and the intermediate five-coordinate geometry (τ = 0.52) which exhibits a typical single broad peak around 12.00-13.00 kK, usually observed for the intermediate five-coordinate geometry. If the distorted trigonal bipyramidal geometry is favorably considered for the intermediate five-coordinate geometry, a single peak which appeared at the lower frequency side of a broad band may be assigned as the d_{xy}, d_{xz}, d_{yz}, $d_{x2-y2} \rightarrow d_{z2}$ transition. In addition, that of the former geometry that appeared at the higher frequency side of a broad band may be assigned as the d_{z2}, d_{xy}, d_{xz}, $d_{yz} \rightarrow d_{x2-y2}$ transition. Both transitions are superimposed to each other resulting in an observed single broad band.

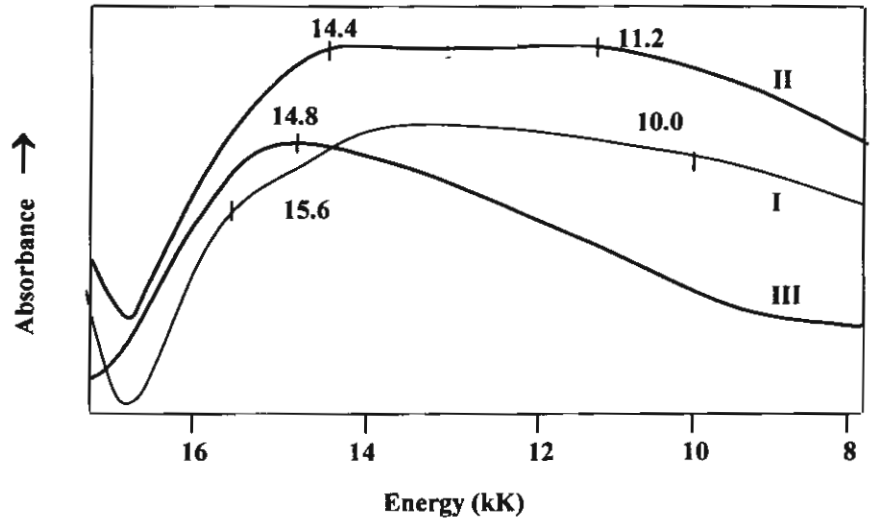

Figure 8 The electronic diffuse reflectance spectra of **I-III**

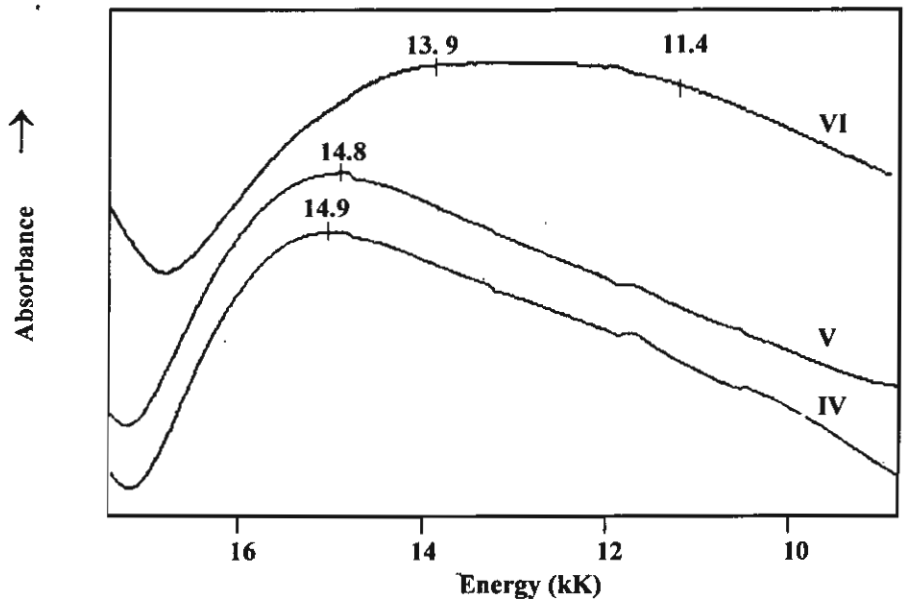

Figure 9 The electronic diffuse reflectance spectra of **IV-VI**

2.4.4 Thermogravimetric analysis

In order to determine the thermal stability of all products, the thermogravimetric analyses of **I-VI** (as in Appendix IID) were carried out in dry air from 30-1000°C using a heating rate of 10°C min^{-1}. The result shows two weight losses, two rather broads. For **I** the first weight loss of about 17.04% occurring in the region 30-300°C corresponds to the loss of hexafluorophosphate anions, dehydration of hydrogenphosphato group and four water molecules (calc. 17.53%) and the second weight loss of 45.24% in the region 300-900°C corresponds to the loss of three amine groups (calc. 46.17%). The final product of the thermal decomposition of **I** is a black powder that appears to be a CuP_2O_7. The thermal behavior of complexes **II** and **III** are given in Appendix IID. The thermogravimetric analysis of **II** and **III** shows two weight losses, two rather broads. The total weight loss of about 53.20% for **II** and 49.40% for **III** occurring in the region 200-850°C corresponds to the loss of water and amine ligand molecules (calc. 54.40% for **II** and 48.40% for **III**, respectively). The final product of the thermal decomposition of **II** and **III** are a black powder that appears to be a CuP_2O_7.

The overall decomposition reactions based on the weight loss data are summarized below:

$$\{[Cu_3(dpyam)_3(\mu_3,\eta^3\text{-}HPO_4)(\mu_3,\eta^4\text{-}PO_4)(H_2O)](PF_6)\cdot 3H_2O\}_n\ (\mathbf{I}) \xrightarrow{-4.5H_2O + PF_6} Cu_3(dpyam)_3P_2O_7 \xrightarrow{-3dpyam} 2\ Cu_2P_2O_7$$

$$[Cu(dpyam)(\mu_2,\eta^3\text{-}HPO_4)]_n\ (\mathbf{II}) \xrightarrow{-1/2H_2O} 1/2\ Cu_2(dpyam)_2P_2O_7 \xrightarrow{-dpyam} 1/2\ Cu_2P_2O_7$$

$$[Cu(dpyam)(\mu_2,\eta^2\text{-}H_2PO_4)(H_2PO_4)]_2\ (\mathbf{III}) \xrightarrow{-4H_2O} Cu_2(dpyam)_2P_2O_7 \xrightarrow{-2dpyam} Cu_2P_2O_7$$

The thermogravimetric analysis of **IV** (as in Appendix IID) shows two weight losses, two rather broads. The first weight loss of about 7.90% occurring in the region 30-100°C corresponds to the loss of twelve water molecules (three from twelve water molecules are considered with site occupancy factor of 0.5, calc. 6.91%) and the second weight loss of 61.90% in the region 150-580°C corresponds to the loss of chloride anions, amine groups and dehydrate of hydrogenphosphato groups (calc. 61.77%). The final product of the thermal decomposition of **IV** is a black powder that appears to be a CuP_2O_7.

The thermal behaviors of complexes **V** and **VI** are given in Appendix IID. The thermogravimetric analysis of **V** is similar to that of complex **IV** suggesting that the total weight loss of about 69.70% corresponds to the loss of water molecules, bromide anions and dehydrate of hydrogenphosphate groups (calc. 71.90%). While complex **VI** shows two weight losses, two rather broads as in the proposed decomposition reactions below. The total weight loss of about 70.30% occurring in the region 100-600°C corresponds to the loss of water and dehydrate of hydrogenphosphate groups, nitrate anions and amine ligand molecules (calc. 70.50%). The final product of the thermal decomposition of **V** and **VI** are also a black powder that appears to be a CuP_2O_7.

The overall decomposition reactions based on the weight loss data are summarized below:

$$2\,[Cu_4(dpyam)_4(\mu\text{-}HPO_4)_2(\mu\text{-}Cl)_2](Cl_2)\cdot 6H_2O\ (\mathbf{IV}) \xrightarrow{-10.5H_2O} 2\,Cu_4(dpyam)_4(HPO_4)_2Cl_4$$

$$\xrightarrow{-8dpyam + 4Cl + 2H_2O} 4\,Cu_2P_2O_7$$

$$2\,[Cu_4(dpyam)_4(\mu\text{-}HPO_4)_2(\mu\text{-}Br)_2](Br_2)\cdot 6H_2O\ (\mathbf{V}) \xrightarrow{-10.5H_2O} 2\,Cu_4(dpyam)_4(HPO_4)_2Br_4$$

$$\xrightarrow{-8dpyam + 4Br + 2H_2O} 4\,Cu_2P_2O_7$$

$$[Cu_4(dpyam)_4(\mu\text{-}HPO_4)_2(H_2O)_2(NO_3)_2](NO_3)_2.2H_2O\ (\mathbf{VI}) \xrightarrow{-4H_2O} Cu_4(dpyam)_4(HPO_4)_2$$

$$(NO_3)_2(NO_3)_2 \xrightarrow{-4dpyam + 4NO_3 + H_2O} 2\,Cu_2P_2O_7$$

2.4.5 EPR spectra

The polycrystalline EPR spectra of $[Cu_3(dpyam)_3(\mu_3,\eta^3\text{-}HPO_4)(\mu_3,\eta^4\text{-}PO_4)(H_2O)](PF_6)\cdot 3H_2O$ (**I**) at both room temperature and liquid nitrogen temperature (77 K) (as in Appendix IIE) are very broad isotropic with g = 2.12 giving no information regarding to the electronic ground state, due to the misalignment of the CuN_2O_2O' chromophores. This single signal can be due to exchange narrowing and also to the compound containing three different copper sites. No half-field signal was observed.

The EPR spectra of complexes **II** and **III** are given in Appendix IIE. The EPR spectrum of compound **II** at room temperature shows an unresolved isotropic signal with g = 2.127. No half-field signal was observed. At liquid nitrogen temperature a more resolved signal is obtained for compound **II** with $g_{//} = 2.291$ and $g_{\perp} = 2.084$. Compound **III** displays an axial signal at both room temperature ($g_{//} = 2.270$ and $g_{\perp} = 2.027$) and liquid nitrogen temperature ($g_{//} = 2.273$ and $g_{\perp} = 2.022$). No triplet signal has been observed. Apparently the dinuclear units in **III** are not isolated from one another, resulting in exchange narrowing. The signals for compounds **II** and **III** are consistent with the d_{x2-y2} ground state and a distorted square-based pyramidal geometry.

The EPR spectra of **IV** (as in Appendix IIE) at both room temperature and liquid nitrogen temperature exhibit four features at 70, 120, 270 and 400 mT and at 50, 110, 250 and 400 mT, respectively. The spectra are qualitatively similar to that reported for other dinuclear copper(II) compounds for other coupled copper(II) pairs with a $|D| > h$. The feature at 270 mT is most

certainly from a mononuclear copper(II) impurity, which is always present in polynuclear species and the weak absorption at low field (120 mT) is the $\Delta M_s = \pm 2$ transition. The presence of the peaks at high field values is as expected when the value of the axial zero-field splitting parameter $|D|$ is larger than the incident quantum (about 0.3 cm^{-1}). At the high-field side (g = 2.004 at both temperatures) a small shoulder is observed, which is due to a signal from the triplet state with a very small zero field splitting, which indicates that there is an interaction between the Cu (II) ions within complex **IV**.

The EPR spectra of complexes **V** and **VI** are also given in Appendix IIE. The EPR spectra of complex **V** is similar to that of complex **IV** suggesting the magnetic interaction between two copper(II) centers in this tetramer. This type of EPR spectrum is also observed in **V**, which shows four features at 60, 135, 270 and 400 mT at room temperature and at 50, 100, 250 and 400 mT at 77 K. While **VI** reveals a very broad isotropic signal with g = 2.13 at room temperature and 77 K giving no information regarding to the electronic ground state, due to the misalignment of the CuN_2O_2O' chromophores. This unresolved signal might be able to be due to exchange narrowing and also to the fact that the compound contains two different copper sites.

2.4.6 Magnetic properties and superexchange mechanism

The magnetic susceptibility of a powdered sample was measured from 5 to 350 K. The magnetic susceptibility plots of $\{[Cu_3(dpyam)_3(\mu_3,\eta^3\text{-}HPO_4)(\mu_3,\eta^4\text{-}PO_4)(H_2O)](PF_6)\cdot 3H_2O\}_n$ **(I)** are depicted in Figs. 10 (a) and (b) in the form of μ_{eff} versus T and χ^{-1} versus T for three Cu(II) ions.

From 350 K to about 30 K the μ_{eff} stays almost constant between 3.1-2.90 BM. This value is lower than the spin-only value of three uncoupled copper(II) S = ½ ions (theoretical value for g = 2, μ_{eff} = 3.88 BM). At about 30 K the μ_{eff} starts to decrease slightly to a value of 1.95 BM at 5 K. This overall behaviour indicates a very weak antiferromagnetic interaction between the Cu(II) ions.

(a)

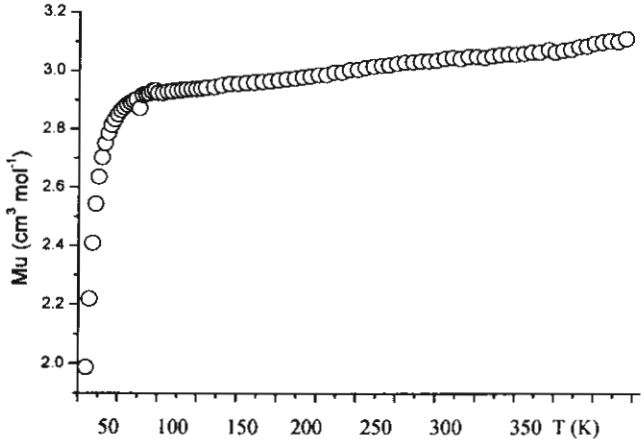

(b)

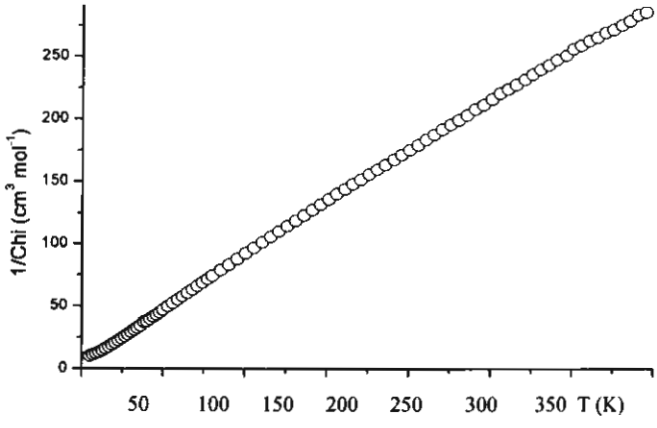

Figure 10 Magnetic susceptibility plot of μ_{eff} versus T (a) and χ^{-1} versus T (b) for compound $[Cu_3(dpyam)_3(\mu_3,\eta^3\text{-}HPO_4)(\mu_3,\eta^4\text{-}PO_4)(H_2O)](PF_6)\cdot 3H_2O\}_n$ **(I)**

The magnetic interaction calculated from Curie-Weiss law out of the χ^{-1} versus T plot, results in a Curie-Weiss constant Θ = -4 K, also indicating a weak antiferromagnetic interaction. This weak interaction can be understood by the fact that the three Cu ions are not equal to each other, the Cu(1) distances to Cu(2) and Cu(3) are large (5.218, 5.942 Å), while the Cu(2)-Cu(3) distance is shorter (4.407 Å), so magnetically it can be also understood as a dinuclear identity which form a polymeric chain via a single Cu ion.

Complex **I** involves both the square pyramidal geometry with an unpaired electron in d_{x2-y2} orbital and an intermediate five-coordinated geometry with an unpaired electron partially delocalized in both d_{x2-y2} and d_{z2} orbitals. In addition, the μ_3,η^3-HPO_4^{2-} and μ_3,η^4-PO_4^{3-} bridges joins copper(II) ions in an equatorial-equatorial and an equatorial-axial configurations between two distorted square pyramidal chromophores and two different geometry chromophores. Hence a weak antiferromagnetic interaction is occurring through the Cu-O-P-O-Cu pathways. The other hydrogenphosphato-bridged complexes with related structures to that of complex **I** are compared as in Table 1.

The magnetic susceptibility plots of complexes **II** and **III** are depicted in Figs 11 and 12 in the form of χ_M and $\chi_M T$ versus T plots. For compound **II**, from 300 K onwards the magnetism is steadily decreasing down to 0.01 $cm^3mol^{-1}K$ at 5 K, indicative for a medium antiferromagnetic coupling between neighbouring Cu(II) ions. The maximum in χ_M, expected for such couplings, is observed at 45 K, and a small Curie tail indicative of paramagnetic impurity is detected below 15 K. The data were fitted using the theoretical expression for a uniform Heisenberg chain. The resulting best fit parameters, corresponding to the full lines were J = -26.20(2) cm^{-1}. For compound **III** the $\chi_M T$ value at 300 K of 0.805 $cm^3mol^{-1}K$, is in agreement with uncoupled spin ½ centres (0.375 $cm^3mol^{-1}K$ per centre with g = 2). Decrease of $\chi_M T$ is observed upon lowering the temperature starting from 50 K down to 0.69 $cm^3\ mol^{-1}K$ at 5 K, which is indicative for a very weak antiferromagnetic interaction. The magnetic data were fitted for two interacting S = ½ centres, based on the general Hamiltonian: $H = -J\ S_1 \cdot S_2$, in which the exchange parameter J is negative for antiferromagetic and positive for ferromagnetic interaction. The data were fitted to the equation given in the literature. Also a Temperature Independent Paramagnetism (TIP) of the Cu(II) ions has been considered. The resulting best fit parameters, corresponding to the full lines were J = -2.85(1) cm^{-1}.

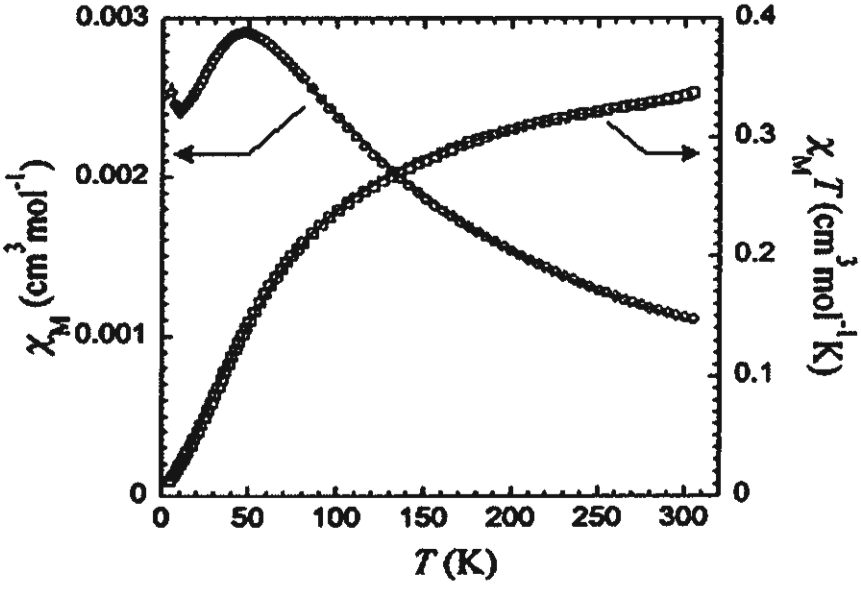

Figure 11 Plots of temperature dependence of the molar magnetic susceptibility χ_M (○) and the $\chi_M T$ product (□) for $[Cu_4(dpyam)_4(\mu_2,\eta^3\text{-}HPO_4)]_n$ **(II)**

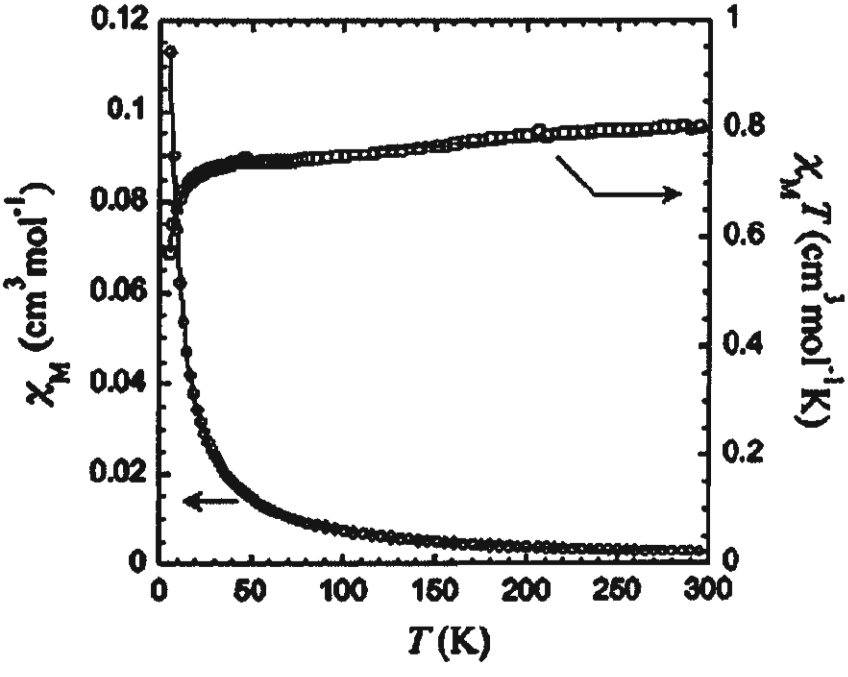

Figure 12 Plots of temperature dependence of the molar magnetic susceptibility χ_M (○) and the $\chi_M T$ product (□) for $[Cu(dpyam)(\mu_2,\eta^2\text{-}H_2PO_4)(H_2PO_4)]_2$ **(III)**

Because of the square pyramidal geometry in compounds **II** and **III** the spin density is mostly in the d_{x2-y2} orbitals of the copper(II) ions. The $H_nPO_4^{(3-n)-}$ bridges, joining the copper atoms in an equatorial-equatorial configuration, the superexchange coupling through the phosphate anion (Cu-O-P-O-Cu) can be expected to be non negligible. The antiferromagnetic couplings found in compounds **II** and **III** are thus in agreement with this structural feature and the large Cu-Cu distances. The compounds together with a number of related complexes **II** and **III** are listed in Table 2 and 3, respectively.

The magnetic susceptibility of a powdered sample for $[Cu_4(dpyam)_4(\mu_4,\eta^3\text{-}HPO_4)_2(\mu\text{-}Cl)_2](Cl)_2\cdot 6H_2O$ **(IV)** was measured from 5 to 350 K. The molar magnetic susceptibility, χ_M, and the product $\chi_M T$ are plotted in Fig. 13.

In this case χ_M gradually increases upon lowering temperature from values at high temperatures in agreement with four uncoupled spin ½ centres. A maximum is reached around 55 K, at which temperature that χ_M decreases sharply. This behaviour is indicative of an antiferromagnetic coupling between some of the copper ions. For simplicity, the two similar tetranuclear units contained in the structure will be considered as identical for the rationalisation of these magnetic properties. Moreover, the diagonal coupling pathways through phosphato groups will also be assumed identical. The magnetic coupling scheme for **IV** proposed in Fig. 14 and the corresponding Hamiltonian writes

$$H = -2J_1(S_A \cdot S_C + S_B \cdot S_D) - 2J_2(S_A \cdot S_B) - 2J_3(S_B \cdot S_C + S_A \cdot S_D) - 2J_4(S_C \cdot S_D) \quad (1)$$

Although the topologies of the compounds differ, this Hamiltonian is identical to one solved for a linear tetranuclear copper compound.

Table 1 Structural and magnetic data of complexes **I-VI** and relevant complexes

[a]*Complex*	*Chromophore*	[b]*Coordination geometry*	[c]τ	[d]*Mode of* $H_xPO_4^{(3-x)-}$	[e]*Bridging configuration*	*J value* (cm^{-1})	*Ref.*
Polynuclear $\{[Cu_3(dpyam)_3(\mu_3,\eta^3\text{-}HPO_4)(\mu_3,\eta^4\text{-}PO_4)(H_2O)](PF_6)\cdot 3H_2O\}_n$ **(I)**	CuN_2O_2O', CuN_2O_3	Dist. SP, TBP	0.17, 0.13, 0.57	3M,3L; 3M,4L	eq-eq, ax-eq	-4.98	This work
$[Cu(dpyam)(\mu,\eta^3\text{-}HPO_4)]_n$ **(II)**	CuN_2O_2O'	dist. SP	0.12	2M,3L	eq-eq, ax-eq	-26.20(2)	This work
$[Cu(phen)(\mu,\eta^2\text{-}HPO_4)(H_2O)_2]_n$ **(1)**	$CuN_2O_2O_2'$	Dist. Oct.	-	2M,2L	ax-ax	-5.86	25
$[Cu_2(bpy)_2(\mu,\eta^2\text{-}HPO_4)(\mu,\eta^1\text{-}H_2PO_4)(\mu,\eta^2\text{-}H_2PO_4)]_n$ **(2)**	CuN_2O_2O'	Dist. SP	0.03, 0.30	2M,2L; 2M,1L	eq-eq, ax-eq	-5.3	26
Dinuclear $[Cu(dpyam)(\mu,\eta^2\text{-}H_2PO_4)(H_2PO_4)]_2$ **(III)**	CuN_2O_2O'	Dist. SP	0,12	1M,1L; 2M,2L	eq-eq	-2.85(1)	This work
Tetranuclear $[Cu_4(dpyam)_4(\mu_4,\eta^3\text{-}HPO_4)_2(\mu\text{-}Cl)_2](Cl)_2\cdot 6H_2O$ **(IV)**	CuN_2O_2O'	Dist. SP	0.020-0.053	4M,3L	eq-eq	22(2), -79(1), 46(4)	This work
$[Cu_4(dpyam)_4(\mu_4,\eta^3\text{-}HPO_4)_2(\mu\text{-}Br)_2](Br)_2\cdot 6H_2O$ **(V)**	CuN_2O_2O'	Dist. SP	0.001-0.071	4M,3L	eq-eq	33(1), -83(1), 12(3)	This work
$[Cu_4(dpyam)_4(\mu_3,\eta^3\text{-}HPO_4)_2(NO_3)_2(H_2O)_2](NO_3)_2\cdot 2H_2O$ **(VI)**	CuN_2O_2O'	Dist. SP, intermediate	0.32^1, 0.49^2	3M,3L	eq-eq, ax-eq	-10.3(1), -5.3(2)	This work
$[Cu_4(phen)_4(\mu_3,\eta^2\text{-}HPO_4)_2(\mu,\eta^2\text{-}H_2PO_4)_2(H_2PO_4)_2].2H_2O$ **(3)**	CuN_2O_2O'	Dist. SP	0.03^1, 0.13^2	1M,1L; 2M,2L; 3M,2L	eq-eq, ax-eq	0.12, -1.32, 0.10	26

[a] Abbreviation: dpyam = di-2-pyridylamine; bpy = 2,2'-bipyridine; phen = 1,10-phenanthroine.
[b] Dist.Oct. = distorted octahedral; Dist.SP = distorted square pyramidal; TBP = trigonal bipyramidal. [c] 1 = Cu(1) chromophore ; 2 = Cu(2) chromophore
[d] M = Metal; L= Ligand [e] ax = axial; eq = equatorial configuration

Table 2 Structural data and electronic spectra of complex **II** and relevant complexes

Complex	Coordination geometry	τ	Chromophore	Tetrago nality	Tetrahedral twist,°	Configuration	J value (cm^{-1})	Ref.
Polymer $[Cu(dpyam)(\mu_3\text{-}HPO_4\text{-}O,O',O'')]_n$ **(II)**	polymeric dist. SP	0.120	CuN_2O_3	0.720	45.5	equatorial-equatorial	-26.20(2)	This work
$Cu(dpyam)(CO_3)]\cdot 3H_2O$ **(1)**	polymeric dist. SP	0.003	$CuN_2O_2O_2'$	0.861	-	axial-equatorial	-	27
$[Cu(dpyam)(H_2O)_2(SO_4)]$ **(2)**	polymeric elong.oct	-	$CuN_2O_2O_2'$	0.815	15.8	axial-axial	-	28
$[Cu(phen)(H_2O)_2(SO_4)]$ **(3)**	polymeric elong.oct	-	$CuN_2O_2O_2'$	0.808	-	axial-axial	-3.8	29
$[Cu(oaoH_2)(H_2O)_2(SO_4)]$ **(4)**	polymeric dist.oct	-	$CuN_2O_2O_2'$	0.832	-	axial-equatorial	-1.0	30
Monomer $[Cu(dpyam)(CO_3)(H_2O)]\cdot 2H_2O$ **(5)**	monomeric dist.SP	0.096	CuN_2O_3	0.899	50.3	-	-	31
$[Cu(tmen)(H_2O)_2(SO_4)]\cdot H_2O$ **(6)**	monomeric dist.SP	0.085	CuN_2O_3	0.908	-	-	-	32
Dimer $[Cu(oaoH_2)(H_2O)(SO_4)]_2$ **(7)**	dinuclear dist.TP	0.145	CuN_2O_3	0.774	-	axial-equatorial	-1.27	30
$[Cu(dpyam)(CO_3)]_2\cdot H_2O$ **(8)**	dinuclear dist.SP	0.220	CuN_2O_3	0.815	5.9[a], 5.1[b]	axial-equatorial	-9.9	33

dpyam = di-2-pyridylamine; bpy = 2,2'-bipyridine; phen = 1,10-phenanthroine; $oaoH_2$; oxamide oxime; tmen = N,N,N',N'-tetramethylethylenediamine; [a]chromophore A ; [b] chromophore B; dist.oct = distorted octahedral; dist.SP = distorted square pyramidal; dist.TP = distorted tetragonal pyramidal

Table 3 Structural data and electronic spectra of complex **III** and relevant complexes

Complex	Coordination geometry	τ	Chromophore	Tetragonality	Tetrahedral twist,°	Bridging configuration	J value (cm^{-1})	Ref.
Dinuclear $[Cu(dpyam)(\mu\text{-}H_2PO_4\text{-}O,O')(H_2PO_4)]_2$ **(III)**	dinuclear SP	0.120	CuN_2O_3	0.874	14.00	equatorial-equatorial	- 2.85(1)	this work
$[Cu(dpyam)(C_6H_3Cl_2OCH_2COO)_2]_2$ **(1)**	dinuclear dist.SP	0.480	CuN_2O_3	0.897	-	axial-equatorial	-0.8	34
$[Cu(dpyam)(ONO\text{-}O,O)(\mu\text{-}ONO\text{-}O)]_2 \cdot 2CH_3CN$ **(2)**	dinuclear dist.SP	0.000	CuN_2O_3	0.813	-	axial-equatorial	-	35
$[Cu_2(dpyam)_2(O_2CH)_4(OH_2)]\cdot H_2O$ **(3)**	dinuclear dist.SP	0.113, 0.096	CuN_2O_3	0.841	16.01,19.35	axial-equatorial	-	36
Monomeric $[Cu(dpyam)(NO_2)_2]$ **(4)**	monomeric dist.oct.	0.020	$CuN_2O_2O_2'$	0.813	31.16	-	-	37
$[Cu(dpyam)(O_2CCH_3)_2]\cdot 2H_2O$ **(5)**	monomeric dist.oct.	-	$CuN_2O_2O_2'$	0.764	34.38	-	-	38
$[Cu(bpy)(NO_3)_2]$ **(6)**	monomeric dist.Oct	-	$CuN_2O_2O_2'$	0.776	27.7	-	-	39
$[Cu(TIMM)(NO_2)_2]$ **(7)**	monomeric dist.Oct	-	$CuN_2O_2O_2'$	0.792	-	-	-	40
$[Cu(BimOBz)(NO_3)_2]$ **(8)**	monomeric dist.Oct	-	$CuN_2O_2O_2'$	0.779	15.6	-	-	41
Polymeric $[Cu(dpyam)(NO_3)_2]$ **(9)**	polymeric elong.oct.	-	$CuN_2O_2O_2'$	0.824, 0.817	7.00, 3.80	-	-	42
$[Cu(dpyam)(NO_3)(O_2CCH_2CH_3)]$ **(10)**	polymeric elong.oct.	-	$CuN_2O_2O_2'$	0.753	-	axial-equatorial	-	43
$[Cu(dpyam)(O_2CCH_3)(O_2ClO_2)]\cdot H_2O$ **(11)**	polymeric elong.oct.	-	$CuN_2O_2O_2'$	0.765	-	axial-axial	-	44

dpyam = di-2-pyridylamine; bpy = 2,2'-bipyridine; TIMM = Tris[2-(1-methyl)imidazolyl]methoxymethane; BimOBz = bis(1-methyl-4,5-diphenylimidaz-2-oyl) (benzyloxy)methane; dist.oct= distorted octahedral; dist.SP = distorted square pyramidal; elong.oct. = elongated octahedral.

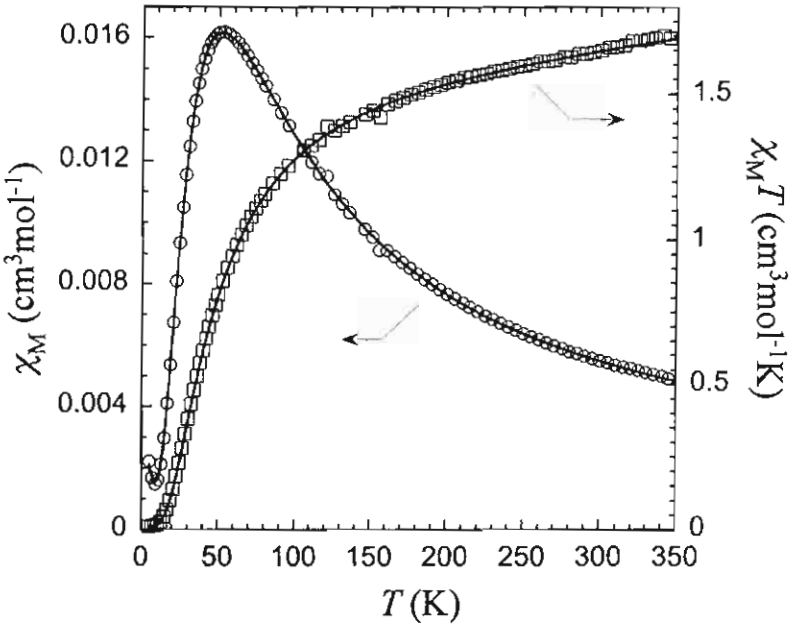

Figure 13 Plots of temperature dependence of the molar magnetic susceptibility χ_M (○) and the $\chi_M T$ product (□) for $[Cu_4(dpyam)_4(\mu_4,\eta^3\text{-}HPO_4)_2(\mu\text{-}Cl)_2](Cl)_2 \cdot 6H_2O$ **(IV)**

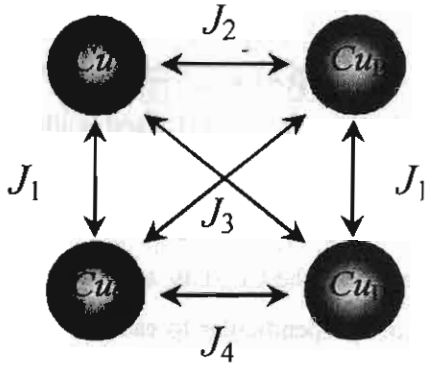

Figure 14 Scheme of the magnetic interactions used in the calculations for $[Cu_4(dpyam)_4(\mu_4,\eta^3\text{-}HPO_4)_2(\mu\text{-}Cl)_2](Cl)_2 \cdot 6H_2O$ **(IV)** and $[Cu_4(dpyam)_4(\mu_4,\eta^3\text{-}HPO_4)_2(\mu\text{-}Br)_2](Br)_2 \cdot 6H_2O$ **(V)**

The energy levels and their spin quantum numbers derived are given in the

$S_1=2$ $E_1=-J_1-J_2/2-J_3-J_4/2$

$S_2=1$ $E_2=J_1-J_2/2+J_3-J_4/2$

$S_3=1$ $E_3=(J_2+J_4)/2+\left[(J_2-J_4)^2+(J_3-J_1)^2\right]^{1/2}$

$S_4=1$ $E_4=(J_2+J_4)/2-\left[(J_2-J_4)^2+(J_3-J_1)^2\right]^{1/2}$

$S_5=0$ $E_5=J_1+J_3+(J_2+J_4)/2+\left[4(J_1^2+J_3^2)+J_2^2+J_4^2-2J_1(J_2+2J_3+J4)-2J_2(J_3-J_4)-2J_3J_4\right]^{1/2}$

$S_6=0$ $E_6=J_1+J_3+(J_2+J_4)/2-\left[4(J_1^2+J_3^2)+J_2^2+J_4^2-2J_1(J_2+2J_3+J4)-2J_2(J_3-J_4)-2J_3J_4\right]^{1/2}$

Considering also that the g values are identical for all copper ions, the molar magnetic susceptibility is then:

$$\chi_M=\frac{N_A g^2\beta^2}{3k_BT}\frac{\sum_i S_i(S_i+1)(2S_i+1)\exp(-E_i/k_BT)}{\sum_i(S_i+1)\exp(-E_i/k_BT)} \qquad (2)$$

A term taking into account a small monomeric paramagnetic impurity was added to this expression and evaluated from the low temperature data as 0.07%. To avoid over-parameterisation, these terms were held constant during the fitting procedure as well as the g value, which was fixed at 2. For this compound, the experimental data were first fitted to eq. 2 letting the coupling constants vary by groups of 2 and 3 and holding the other(s) to 0. This way, it was found first that $2J_3$ had to be negative of the order of -90 K, and second, that the other coupling constants should be positive with J_1 and J_2 of the same order, to obtain a good fit. At this point one has to remark that apart for the Cu_A-Cu_C and Cu_B-Cu_D pairs, the basal planes of the other pairs of copper ions are almost perpendicular to each other. This indicates that the overlap between the spin-rich d_{x2-y2} orbitals of these copper ions cannot be expected to be important. In addition, Cu_C-O-Cu_D angles are close to 90°, value yielding ferromagnetic interaction in alkoxo- or hydroxo- bridged copper dimers. Finally, chloride bridges between Cu_A and Cu_B and Cu_C and Cu_D respectively correspond to the axial coordination site of the copper ions where the spin density is negligible. Therefore, the participation of this pathway to the interactions should be negligible.

Hence the data were then fit by forcing $J_1 = J_2$ and letting the three remaining coupling constants free, starting from $J_3<0$ and J_1 and $J_4>0$. The two sets of best fit parameters,

corresponding to the full lines in Fig. 13, were obtained as $2J_1 = 2J_2 = 22(1)$ cm^{-1}, $2J_3 = -79.4(7)$ cm^{-1}, $2J_4 = 46(3)$ cm^{-1}. This concludes that the compound presents a singlet ground state with a first excited triplet state at E_4-E_6 (eg. 76 cm^{-1}) above it. The molar magnetic susceptibilities of complexes **V** and **VI** are depicted in Figs. 15 and 16.

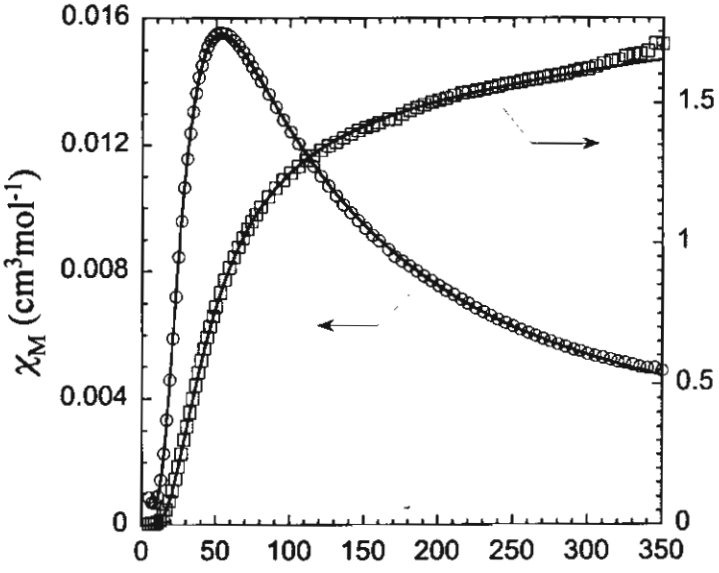

Figure 15 Plots of temperature dependence of the molar magnetic susceptibility χ_M (○) and the $\chi_M T$ product (□) for $[Cu_4(dpyam)_4(\mu_4,\eta^3\text{-}HPO_4)_2(\mu\text{-}Br)_2](Br)_2 \cdot 6H_2O$ **(V)**

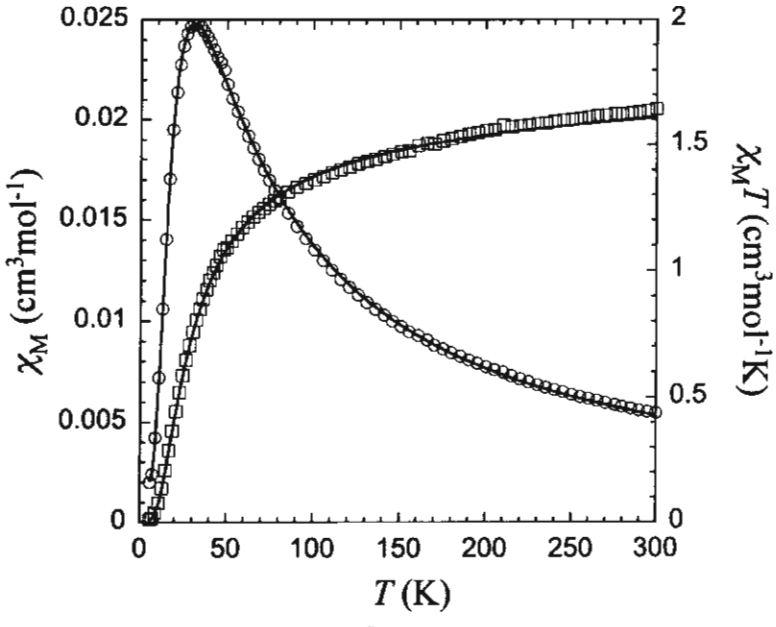

Figure 16 Plots of temperature dependence of the molar magnetic susceptibility χ_M (○) and the $\chi_M T$ product (□) for $[Cu_4(dpyam)_4(\mu_3,\eta^3\text{-}HPO_4)_2(NO_3)_2(H_2O)_2](NO_3)_2 \cdot 2H_2O$ **(VI)**

Compound **V** is isostructural with compound **IV** and involves a similar asymmetric unit and similar distorted square pyramidal geometry. Hence the data were then fit by forcing $J_1 = J_2$ and letting the three remaining coupling constants free, starting from $J_3<0$ and J_1 and $J_4>0$. The two sets of best fit parameters, corresponding to the full lines were obtained as $2J_1 = 2J_2 = 33.3(7)$ cm^{-1}, $2J_3 = -83.1(5)$ cm^{-1}, $2J_4 = 12(2)$ cm^{-1}. This concludes that the compound presents a singlet ground state with a first excited triplet state at E_4-E_6 (and 84 cm^{-1}) above it.

Fig. 17 shows the magnetic interaction scheme of **VI**, which was used for the fitting procedure and is based on the assumption that the magnetic coupling of the outer Cu ions (Cu(1)-Cu(2), Cu(1)-Cu(2A)) is identical. This is understandable as the main difference lies in a long Cu-O apical bond, where no spin density is expected. The corresponding Hamiltonian is then :

$$H = -J_1\left(S_1 \cdot S_2 + S_1 \cdot S_{2'} + S_{1'} \cdot S_2 + S_{1'} \cdot S_{2'}\right) - J_2\left(S_2 \cdot S_{2'}\right)$$

Applying the Kambe vector coupling method with $S_A = S_1+S_{1'}$ and $S_B = S_2+S_{2'}$ (1 is for outer magnetic Cu-Cu interaction and 2 for inner magnetic Cu-Cu interaction, see Fig. 17) yields the following expression for the energy levels:

$$E(S_T,S_A,S_B)=-\frac{J_1}{2}\left(S_T(S_T+1)-S_A(S_A+1)-S_B(S_B+1)\right)-\frac{J_2}{2}\left(S_B(S_B+1)\right)$$

and after inserting in the van Vleck equation the expression for the molar susceptibility :

$$\chi_{tetra}=(1-p)\frac{Ng^2\beta^2}{k_BT}\frac{\left[2+2\exp\left(\frac{J_2}{k_BT}\right)+10\exp\left(\frac{(J_1+J_2)}{k_BT}\right)\right]}{\left[4+3\exp\left(\frac{J_2}{k_BT}\right)+5\exp\left(\frac{(J_1+J_2)}{k_BT}\right)+\exp\left(\frac{-2J_1+J_2}{k_BT}\right)\right]}+\frac{4\times0.375\times p}{T}+TIP$$

which includes terms to take into account: Temperature Independent Paramagnetism (TIP) and a monomeric paramagnetic impurity (p). Fitting the experimental data to this expression yields the full lines corresponding to the parameters g = 1.99(1), J_1 = -20.4(1) cm^{-1}, J_2 = -10.1(2) cm^{-1}. In light of the longer distance of the inner Cu-Cu ions (Cu(1)-Cu(1A)) in contrary to the outer Cu-Cu distance (Cu(1)-Cu(2)), the found J values seem to be reasonable.

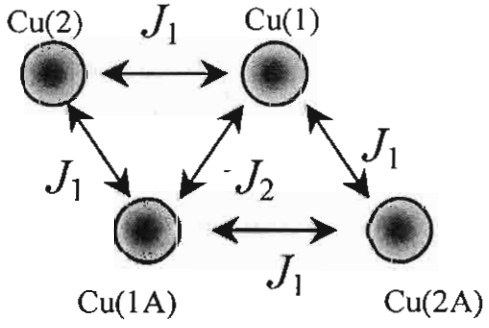

Figure 17 Scheme of the magnetic interactions used in the calculations for $[Cu_4(dpyam)_4(\mu_3,\eta^3\text{-}HPO_4)_2(NO_3)_2(H_2O)_2](NO_3)_2\cdot2H_2O$ **(VI)**

Because of the square pyramidal geometry in compounds **IV** and **V** the spin density is mostly in the $d_{x^2-y^2}$ orbitals of the copper(II) ions. The $H_nPO_4^{(3-n)-}$ bridges join the copper atoms in an equatorial-equatorial configuration, the superexchange coupling through the phosphate anion (Cu-O-P-O-Cu) can be expected to be non negligible. The antiferromagnetic couplings found in compounds **IV** and **V** are thus in agreement with this structural feature and the large Cu-Cu distances. The magnetic susceptibility measurements (5-350 K) reveal an antiferromagnetic interaction. While the phosphate bridges in compound **VI** join the copper atoms in an equatorial-equatorial and an equatorial-axial modes between two distorted square pyramidal chromophores

with an unpaired electron in $d_{x^2-y^2}$ orbital and link the copper atoms in an axial-equatorial mode between an intermediate five-coordinate chromophore and a distorted square pyramidal chromophore with an unpaired electron partially delocalized in both $d_{x^2-y^2}$ and d_{z^2} orbitals for an intermediate five-coordinate chromophore. Hence, a weak antiferromagnetic interaction is occurring through the Cu-O-P-O-Cu pathways.

2.5 Conclusions

The second part of this research sets out to examine and develop the preparative work of a series of polynuclear hydrogenphosphato-bridged copper(II) complexes with di-2-pyridylamine (dpyam) ligand. The spectroscopic and magnetic characterization, the crystal structure determination and the magneto-structural correlation of this complex system are investigated and discussed.

The polynuclear hydrogenphosphato-bridged copper(II) complexes $\{[Cu_3(dpyam)_3(\mu_3,\eta^3\text{-}HPO_4)(\mu_3,\eta^4\text{-}PO_4)(H_2O)](PF_6)\cdot 3H_2O\}_n$ **(I)**, $[Cu(dpyam)(\mu_2,\eta^3\text{-}HPO_4)]_n$ **(II)**, $[Cu(dpyam)(\mu_3,\eta^3\text{-}H_2PO_4)(H_2PO_4)]_2$ **(III)**, $[Cu_4(dpyam)_4(\mu_4,\eta^3\text{-}HPO_4)_2(\mu\text{-}Cl)_2](Cl)_2\cdot 6H_2O$ **(IV)**, $[Cu_4(dpyam)_4(\mu_4,\eta^3\text{-}HPO_4)_2(\mu\text{-}Br)_2](Br)_2\cdot 6H_2O$ **(V)** and $[Cu_4(dpyam)_4(\mu_3,\eta^3\text{-}HPO_4)_2(NO_3)_2(H_2O)_2](NO_3)_2\cdot 2H_2O$ **(VI)** were prepared directly from the mole ratio in various solvents. All products were analyzed by elemental microanalyses and TG-DTA and characterized spectroscopically (IR, EPR, solid state and VIS). The X-ray crystal structures of all products are determined and reported in details in comparison with those of the related complexes.

Complexes **I** and **II** exhibit polymeric chains of the $[Cu_3(dpyam)_3(\mu_3,\eta^3\text{-}HPO_4)(\mu_3,\eta^4\text{-}PO_4)(H_2O)]^+$ cation and $[Cu(dpyam)(\mu_2,\eta^3\text{-}HPO_4)]$ unit, respectively with the novel bridging coordination modes $\mu_3,\eta^3\text{-}HPO_4$ and $\mu_3,\eta^4\text{-}PO_4$ for **I** and $\mu_2,\eta^3\text{-}HPO_4$ for **II**. The trimeric unit in **I** involves two CuN_2O_2O' chromophores with a tetrahedrally distorted square-based pyramidal geometry (τ = 0.17 and 0.13) and a CuN_2O_3 chromophore with an intermediate five-coordinate geometry (τ = 0.57). Complex **II** displays a distorted square-based pyramidal geometry of the CuN_2O_2O' chromophore with τ = 0.12. Complex **III** is a dinuclear compound consisting of the $\mu_2,\eta^2\text{-}H_2PO_4$ bridge and the monodentate H_2PO_4 group with a distorted square pyramidal CuN_2O_2O' chromophore (τ = 0.12). Complexes **IV**, **V** and **VI** are tetranuclear compounds consisting of the tetrameric units $[Cu_4(dpyam)_4(\mu_4,\eta^3\text{-}HPO_4)_2(\mu\text{-}Cl)_2]^{2+}$, $[Cu_4(dpyam)_4(\mu_4,\eta^3\text{-}HPO_4)_2(\mu\text{-}Br)_2]^{2+}$ and $[Cu_4(dpyam)_4(\mu_3,\eta^3\text{-}HPO_4)_2(NO_3)_2(H_2O)_2]^{2+}$, respectively. Complexes **IV** and **V** are isostructural, both having the $\mu_4,\eta^3\text{-}HPO_4$ bridging coordination mode with the halide bridges. Each copper(II) environment involves a range of the distorted square pyramidal geometry of CuN_2O_2X chromophores with τ = 0.02-0.05 for **IV** and τ = 0.001-0.07 for **V**. Complex **VI** exhibits two different geometries, a tetrahedrally distorted square-based pyramid (τ = 0.32) of two CuN_2O_2O' chromophores and an intermediate five-coordinate geometry

(τ = 0.52) of the other two CuN_2O_3 chromophores with an unprecedented μ_4,η^3-HPO_4 bridging coordination mode.

The magnetic interaction in **I** calculated from Curie-Weiss law out of the χ^{-1} versus T plot, results in a Curie-Weiss constant Θ = -4 K, also indicating a weak antiferromagnetic interaction. This weak interaction can be understood by the fact that the three Cu ions are not equal to each other, the Cu(1) distances to Cu(2) and Cu(3) are large (5.218, 5.942 Å), while the Cu(2)-Cu(3) distance is shorter (4.407 Å), so magnetically it can be also understood as a dinuclear identity which form a polymeric chain via a single Cu ion. Compounds **II** and **III** have the singlet-triplet energy gaps J = -26.20(2) and -2.85(1) cm^{-1}, respectively, which confirm the medium and weak antiferromagnetic interactions, respectively between neighboring Cu(II) ions. Because of the square pyramidal geometry in **II** and **III** the spin density is mostly in the d_{x2-y2} orbitals of the copper(II) ions. Although the $H_nPO_4^{(3-n)-}$ bridges, join the copper atoms in an equatorial-equatorial configuration, both square bases are not parallel in the same plane with an anti-anti or syn-anti configuration of the $H_nPO_4^{(3-n)-}$ bridges. Consequently, the superexchange coupling through the phosphate anion (Cu-O-P-O-Cu) can be expected to be non negligible. The antiferromagnetic couplings found in **II** and **III** are thus in agreement with this structural feature and the large Cu-Cu distances. Compound **IV** has the singlet-triplet energy gaps $2J_1 = 2J_2 = 22(1)$ cm^{-1}, $2J_3 = -79.4(7)$ cm^{-1}, $2J_4 = 46(3)$ cm^{-1} for different pathways. Those of **V** are $2J_1 = 2J_2 = 33.3$ (7) cm^{-1}, $2J_3 = -83.1(5)$ cm^{-1}, $2J_4 = 12(2)$ cm^{-1}. This concludes that both compounds present a singlet ground state. Compound **VI** has the singlet-triplet energy gaps $J_1 = -20.4(1)$ cm^{-1} and $J_2 = -10.1(2)$ cm^{-1}. In light of the longer distance of the inner Cu-Cu ions (Cu(1)-Cu(2)), the found J values seem to be reasonable. The phosphate bridges in **VI** join copper atoms in an equatorial-equatorial modes between two distorted square pyramidal chromophores which have a marked tetrahedral twist of the square bases and the large Cu-Cu distance and link the copper atoms in the equatorial-axial and axial-axial configuration modes between two different geometries (τ = 0.32 and 0.52). The antiferromagnetic interaction found in **VI** is thus in agreement with this structural feature.

The results of all products obtained in this complex series have been published[25, 45-49].

References

1. Lii K.-H, Huang Y.-F, Zima V, Huang C.-Y, Lin H.-M, Jiang Y.-C, Liao F.-L, Wang S.-L. ***Chem. Mater.*** 1998; 10: 2599.
2. Cheetham A.K, Férey G, Loiseau T. ***Angew. Chem. Int. Ed.*** 1999; 38: 3268.
3. Kitagawa S, Kondo M. ***Bull. Chem. Soc. Jpn.*** 1998; 71: 1739.
4. Chui S.S.-Y, Lo S.M.-F, Charmant J. P.H, Orpen A.G, Williams I.D. ***Science*** 1999; 283: 1148.
5. Kagan C. R, Mitzi D. B, Dimitrakopoulos C. D. ***Science*** 1999; 286: 945.
6. Batten S. R, Robson R. ***Angew. Chem., Int. Ed. Engl.*** 1998; 37: 1460.
7. Zaworotko M. J. ***Angew. Chem., Int. Ed. Engl.*** 1998; 37: 1211.
8. Hagrman D, Hammond R.P, Haushalter R.C, Zubieta J. ***Chem. Mater.*** 1998; 10: 2091.
9. Hagrman P.J, Hagrman D, Zubieta J. ***Angew. Chem. Int. Ed.*** 1999; 38: 2638.
10. Choudhury A, Natarajan S, Rao C.N.R. ***J. Solid State Chem.*** 1999; 146: 538.
11. Choudhury A, Natarajan S. ***J. Mater. Chem.*** 1999; 9: 3113.
12. Choudhury A, Natarajan S, Rao C.N.R. ***Chem.-A Eur. J.*** 2000; 6: 1168.
13. Chang W.-J, Lin H.-M, Lii K.-H. ***J. Solid State Chem.*** 2000; 157: 233.
14. Tsai Y.-M, Wang S.-L, Huang C.-H, Lii K.-H. ***Inorg. Chem.*** 1999; 38: 4183.
15. Do J, Bontchev R.P, Jacobson A.J. ***Chem. Mater.*** 2001; 13: 2601.
16. Finn R.C, Zubieta J. ***J. Phy. Chem. Solids.*** 2001; 62: 1513.
17. Zhang X.-M, Tong M.-L, Feng S.-H, Chen X.-M. ***J. Chem. Soc. Dalton Trans.*** 2001; 2069.
18. Finn R.C, Zubieta J. ***J. Chem. Soc. Dalton Trans.*** 2000; 16: 856.
19. Zhang X.-M, Wu H.-S, Gao S, Chen X.-M. ***J. Solid State Chem.*** 2003; 176: 69.
20. Chang W.-J, Chen C.-Y, Lii K.-H. ***J. Solid State Chem.*** 2003; 172: 6.
21. Lin Z.-E, Zhang J, Sun Y.-Q, Yang G.-Y. ***Inorg. Chem.*** 2004; 43: 797.
22. Zhang Y, Haushalter R.C, Zubieta J. ***Inorg. Chim. Acta.*** 1997; 260: 105.
23. Lin C.-H, Wang S.-L. ***Inorg. Chem.*** 2001; 40: 2918.
24. Lu Y, Wang E, Yuan M, Luan G, Li Y, Zhang H, Hu C, Yao Y, Qin Y, Chen Y. ***J. Chem. Soc. Dalton Trans.*** 2000; 3029.
25. Youngme S, Phuengphai P, Pakawatchai C, van Albada GA, Tanase S, Mutikainen I, Turpeinen U, Reedijk J. ***Inorg. Chem. Commun.*** 2005; 8: 335.
26. Youngme S, Phuengphai P, Pakawatchai C, van Albada GA, Tanase S, Mutikainen I, Turpeinen U, Reedijk J. ***Polyhedron*** 2006; inpress.

27. Sletten J, ***Acta Chem. Scand., Sect. A*** 1984; 38: 491.
28. Youngme S, Chaichit N, Pakawatchai C, Booncoon S, ***Polyhedron*** 2002; 21: 1279.
29. Xu L, Wang E, Peng J, Huang R. ***Inorg. Chem. Commun.*** 2003; 6: 740.
30. Endres H, Nöthe D, Rossato E, Hatfield WE. ***Inorg. Chem.*** 1984; 23: 3467.
31. Akhter P, Fitzsimons P, Hathaway B. ***Acta Crystallogr., Sect. C*** 1991; 47 308.
32. Balvich J, Fivizzani KP, Pavkovic SF, Brown JN. ***Inorg. Chem.*** 1976; 15 71.
33. Youngme S, Chaichit N, Kongsaeree P, van Albada GA, Reedijk J. ***Inorg. Chim. Acta*** 2001; 20: 232.
34. Psomas G, Raptopoulou CP, Iordanidis L, Dendrinou- Samara C, Tangoulis V, Kessissoglou DP. ***Inorg. Chem.*** 2000; 39: 3042.
35. Camus A, Marsich N, Lanfredi AMM, Ugozzoli F, Massera C. ***Inorg. Chim. Acta*** 2000; 309: 1.
36. Youngme S, Somjitsripunya W, Chinnakali K, Chantrapromma S, Fun HK. ***Polyhedron*** 1999; 18: 857.
37. Youngme S, Tonpho S, Chinnakali K, Chantrapromma S, Fun HK. ***Polyhedron*** 1999; 18: 851.
38. Youngme S, Pakawatchai C, Fun HK, Chinnakali K. ***Acta Crystallogr., Sect. C*** 1998; 54: 1586.
39. Tadsanaprasittipol A, Kraatz HB, Enright GD. ***Inorg. Chim. Acta*** 1998; 278: 143.
40. Stibrany RT, Potenza JA, Schugar HJ. ***Inorg. Chim. Acta*** 1996; 243: 33.
41. Bhalla R, Helliwell M, Garner CD. ***Inorg. Chem.*** 1997; 36: 2944.
42. Youngme S, Chaichit N, Damnatara K. ***Polyhedron*** 2002; 21: 943.
43. Youngme S, Pakawatchai C, Fun HK. ***Acta Crystallogr., Sect. C*** 1998; 54: 451.
44. Ray N, Tyagi S, Hathaway BJ. ***Acta Crystallogr., Sect. B*** 1982; 38: 1574.
45. Youngme S, Phuengphai P, Chaichit N, Pakawatchai C, van Albada GA, Roubeau O, Reedijk J. ***Inorg. Chim. Acta*** 2004; 357: 3603.
46. Youngme S, Phuengphai P, Pakawatchai C, van Albada GA, Roubeau O, Reedijk J. ***Inorg. Chim. Acta*** 2005; 358: 849.
47. Youngme S, Phuengphai P, Chaichit N, Pakawatchai C, van Albada GA, Reedijk J. ***Inorg. Chim. Acta*** 2005; 358: 2125.
48. Youngme S, Phuengphai P, Chaichit N, van Albada GA, Roubeau O, Reedijk J. ***Inorg. Chim. Acta*** 2005; 358: 2262.

49. Phuengphai P, Youngme S, Pakawatchai C, van Albada GA, Quesada M, Reedijk J. ***Inorg. Chem. Commun.*** 2005; 9: 147.

Part III

Synthesis, Crystal Structure, Spectroscopic and Magnetic Properties of Dinuclear Formato-bridged Copper(II) Compounds

3

Synthesis, Crystal Structure, Spectroscopic and Magnetic Properties of Dinuclear Formato-Bridged Copper(II) Compounds

3.1 Introduction

The triply-bridged dinuclear copper(II) carboxylato complexes involving didentate chelate ligand are reported in the literature[1-14]. These complexes exhibit many types of bridging conformations of the carboxylato bridges (Fig. 1) and various geometries of copper(II) ions. The previous reports have established that the type (antiferromagnetic or ferromagnetic) and magnitude of magnetic exchange interaction are influenced by the bridge identity, the coordination geometry of copper(II) ion, the Cu···Cu separation, the bond angles at the bridging atoms, the dihedral angle between the planes containing the copper(II) ions and the copper-bridging ligand bond lengths[3]. Among the copper(II) carboxylato complexes, the copper(II) acetates form a large family with many structurally characterized complexes for which magnetic and spectroscopic properties have been measured. In contrast, a closely related structure in formate and propionate families is rarely reported. Because of the variety of the geometries displayed by the copper(II) ion and also because of the structurally dependent magnetic properties, an attempt has been made to prepare the copper(II) complexes containing the chelate di-2-pyridylamine (dpyam) ligand and involving the formato bridge. The triply-bridged dinuclear copper(II) complexes $[Cu_2(dpyam)_2(\mu\text{-}O_2CH)(\mu\text{-}OH)(\mu\text{-}OCH_3)](ClO_4)$ **(I)**, $[Cu_2(dpyam)_2(\mu\text{-}O_2CH)(\mu\text{-}OH)_2](ClO_4)\cdot H_2O$ **(II)**, $[Cu_2(dpyam)_2(\mu\text{-}O_2CH)(\mu\text{-}OOCH)(\mu\text{-}OH)](PF_6)$ **(III)**, $[Cu_2(dpyam)_2(\mu\text{-}O_2CH)(\mu\text{-}OH)(\mu\text{-}Cl)](ClO_4)\cdot 0.5H_2O$ **(IV)**, $[Cu_2(dpyam)_2(\mu\text{-}O_2CH)(\mu\text{-}OH)(\mu\text{-}Cl)](PF_6)$ **(V)** and $[Cu_2(dpyam)_2(\mu\text{-}O_2CH)(\mu\text{-}OH)(\mu\text{-}Cl)](BF_4)$ **(VI)** are reported.

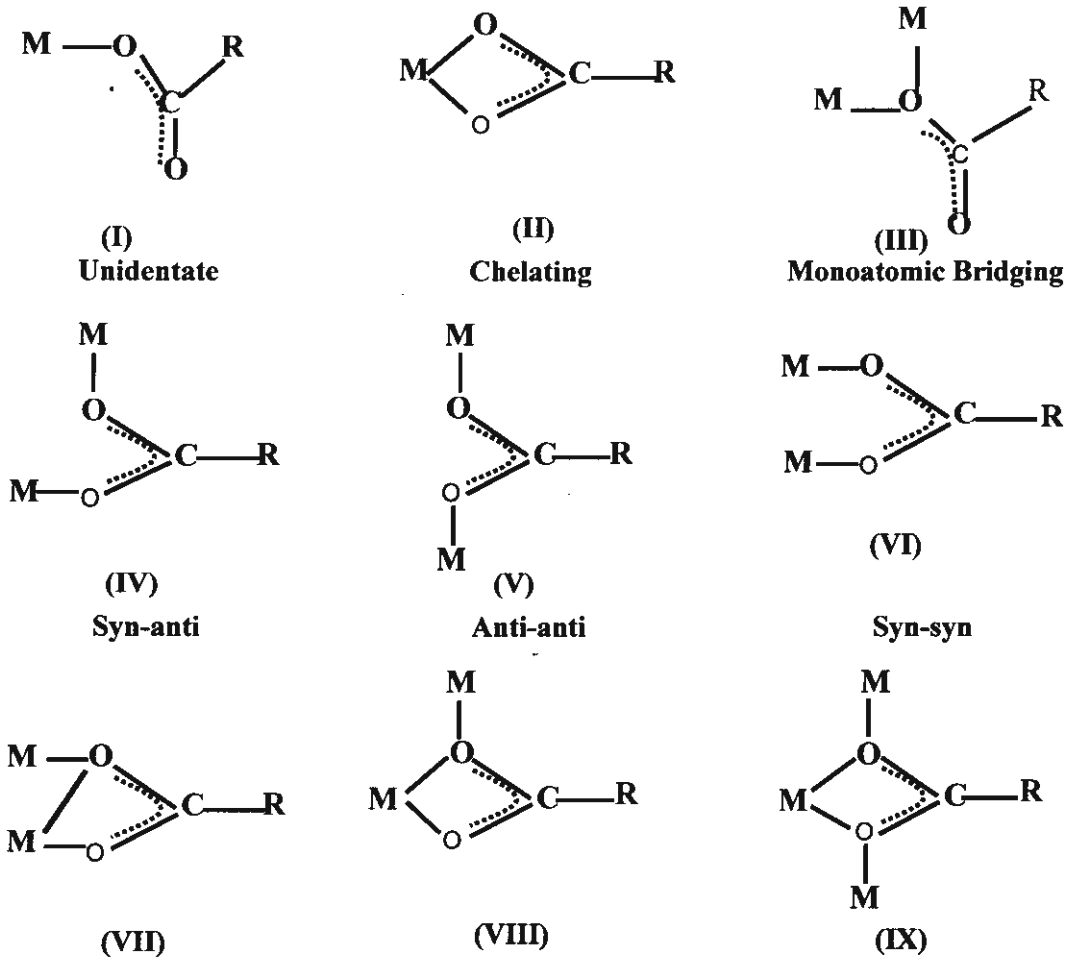

Figure 1 Different coordination modes of carboxylato ligand

3.2 Aims and Scopes

The objective of the third part of this research is to examine and develop the preparation work of the dinuclear copper(II) complexes containing the formate as a bridging ligand and the di-2-pyridylamine as a chelate didentate terminal ligand. The products are characterized by elemental analyses and their spectroscopic properties (IR, solid state VIS, EPR (room temperature and liquid nitrogen temperature)). The molecular and crystal structures were determined by X-ray diffraction method. The room temperature magnetic moment and the temperature variable susceptibilities (5-350 K) were measured and the magneto-structural correlation together with the superexchange pathways are investigated and discussed in comparison with other relevant complexes.

3.3 Experimental

3.3.1 Reagents and physical measurements

All reagents are commercial grade materials and were used without further purification. Elemental analyses(C, H, N) were performed by the Microanalytical Service of Science and Technological Research Equipment Center, Chulalongkorn University on Perkin-Elmer PE2400 CHNS/O Analyzer. Copper content was determined on atomic absorption spectrophotometer. IR spectra were recorded with a Biorad FTS-7/PC FTIR spectrophotometer as KBr pellets/and or as nujol mulls in the 4000 – 450 cm^{-1} spectral range. Solid-state (diffuse reflectance) electronic spectra were recorded as polycrystalline samples on a Perkin-Elmer Lambda2S spectrophotometer over the range 8000–18000 cm^{-1}. X-band powder EPR spectra were obtained on a Jeol RE2x electron spin resonance spectrometer using DPPH (g = 2.0036) as a standard. Magnetic susceptibility measurements (5-280 K) were carried out using a Quantum Design MPMS-5 5T SQUID magnetometer (measurements carried out at 1000 Gauss). Data were corrected for magnetization of the sample holder and for diamagnetic contributions, which were estimated from the Pascal constants.

3.3.2 Syntheses

$[Cu_2(dpyam)_2(\mu\text{-}O_2CH)(\mu\text{-}OH)(\mu\text{-}OCH_3)](ClO_4)$ (I)

A hot methanol solution (10 ml) containing dpyam (0.171 g, 1.0 mmol) was added to a hot aqueous solution (10 ml) of $Cu(ClO_4)_2{\cdot}6H_2O$ (0.371 g, 1.0 mmol), after which solid HCOONa (0.272 g, 4.0 mmol) was added. The resulting green solution was allowed to evaporate at room temperature. After one week, green polygon-shape crystals of **I** were obtained which were filtered off, washed with the mother liquid and air-dried. Yield ca. 80%. Calc. for $[Cu_2(dpyam)_2(\mu\text{-}O_2CH)(\mu\text{-}OH)(\mu\text{-}OCH_3)](ClO_4)$ **(I)**: C, 39.92; H, 3.50; N, 12.70; Cu, 19.20%. Found: C, 39.80; H, 3.62; N, 12.90; Cu, 18.99%.

$[Cu_2(dpyam)_2(\mu\text{-}O_2CH)(\mu\text{-}OH)_2](ClO_4){\cdot}H_2O$ (II)

A hot methanol solution (10 ml) of dpyam (0.171 g, 1.0 mmol) was added to a hot aqueous solution (20 ml) of $Cu(COOH)_2$ (0.154 g, 1.0 mmol). Then a solid of HCOONa (0.204 g, 3.0 mmol) was added, followed by a solid of $NaClO_4$ (0.195 g, 1.0 mmol). The green powder immediately formed, after which the mixture was warmed and the methanol solution (10 ml) and the aqueous solution (10 ml) were added, yielding a clear green solution. On slow evaporation at room temperature for two weeks, the product **II** was isolated as blue rod-shape crystals. They were filtered off, washed with the mother liquid and air-dried. Yield

ca. 30%. Calc. for $[Cu_2(dpyam)_2(\mu\text{-}O_2CH)(\mu\text{-}OH)_2](ClO_4)\cdot H_2O$ **(II)**: C, 37.87; H, 3.48; N, 12.62; Cu, 19.08%. Found: C, 37.59; H, 3.33; N, 12.53; Cu, 18.87%.

$[Cu_2(dpyam)_2(\mu\text{-}O_2CH)(\mu\text{-}OOCH)(\mu\text{-}OH)](PF_6)$ (III)

This complex was prepared by adding a hot DMSO solution (5 ml) of dpyam (0.171 g, 1.0 mmol), to a hot aqueous solution (10 ml) of $Cu(COOH)_2$ (0.154 g, 1.0 mmol), after which a hot methanol solution (10 ml) of KPF_6 (0.184 g, 1.0 mmol) was added. The resulting green solution was allowed to evaporate at room temperature. After two weeks, green hexagon-shape crystals of **III** were obtained which were filtered off, washed with the mother liquid and air-dried. Yield ca. 75%. Calc. for $[Cu_2(dpyam)_2(\mu\text{-}O_2CH)(\mu\text{-}OOCH)(\mu\text{-}OH)](PF_6)$: C, 36.62; H, 2.93; N, 11.65; Cu, 17.62%. Found: C, 36.13; H, 2.58; N, 11.81; Cu, 17.12%.

$[Cu_2(dpyam)_2(\mu\text{-}O_2CH)(\mu\text{-}OH)(\mu\text{-}Cl)](ClO_4)\cdot 0.5H_2O$ (IV)

A hot DMF solution (20 ml) of dpyam (0.171 g, 1.0 mmol) was added to a hot aqueous solution (10 ml) of $CuCl_2\cdot 2H_2O$ (0.171 g, 1.0 mmol). Then a hot aqueous solution (10 ml) of HCOONa (0.136 g, 2.0 mmol) was added to the mixture yielding a dark green solution, after which the solid $KClO_4$ (0.416 g, 3.0 mmol) was added. The resulting green solution was allowed to evaporate at room temperature. After a month, green polygon-shape crystals of **IV** were formed which were filtered off, washed with the mother liquid and air-dried. Yield ca. 75%. Calc. for $[Cu_2(dpyam)_2(\mu\text{-}O_2CH)(\mu\text{-}OH)(\mu\text{-}Cl)](ClO_4)\cdot 0.5H_2O$: C, 37.34; H, 3.13; N, 12.44; Cu, 18.82%. Found: C, 37.66; H, 3.40; N, 12.50; Cu, 18.49%.

$[Cu_2(dpyam)_2(\mu\text{-}O_2CH)(\mu\text{-}OH)(\mu\text{-}Cl)](PF_6)$ (V)

A hot DMF solution (10 ml) of dpyam (0.171 g, 1.0 mmol) was added to a hot DMF solution (10 ml) of $CuCl_2\cdot 2H_2O$ (0.171 g, 1.0 mmol). Then solid HCOONa (0.136 g, 2.0 mmol) was added to the mixture yielding a brown solution. Its color became green by addition of an aqueous solution (5 ml) of KPF_6 (0.184 g, 1.0 mmol). After a month, green hexagon-shape crystals of **V** were obtained, which were filtered off, washed with the mother liquid and air-dried. Yield ca. 81%. Calc. for $[Cu_2(dpyam)_2(\mu\text{-}O_2CH)(\mu\text{-}OH)(\mu\text{-}Cl)](PF_6)$ **(V)**: C, 35.43; H, 2.83; N, 11.81; Cu, 17.85%. Found: C, 35.65; H, 2.71; N, 11.61; Cu, 17.71%.

$[Cu_2(dpyam)_2(\mu\text{-}O_2CH)(\mu\text{-}OH)(\mu\text{-}Cl)](BF_4)$ (VI)

This complex was prepared by adding a hot DMF solution (10 ml) of dpyam (0.171 g, 1.0 mmol) to a hot aqueous solution (10 ml) of $CuCl_2\cdot 2H_2O$ (0.171 g, 1.0 mmol), then an aqueous solution (5 ml) of HCOONa (0.136 g, 2.0 mmol) was added. The resultant solution was then warmed and a solid of $NaBF_4$ (0.329 g, 3.0 mmol) was added. The resulting green solution was allowed to evaporate at room temperature. After two weeks, green polygon-

shape crystals of **VI** were formed which were filtered off, washed with the mother liquid and air-dried. Yield ca. 76%. Calc. for $[Cu_2(dpyam)_2(\mu\text{-}O_2CH)(\mu\text{-}OH)(\mu\text{-}Cl)](BF_4)$: C, 38.58; H, 3.08; N, 12.85; Cu, 19.44%. Found: C, 38.11; H, 3.24; N, 12.57; Cu, 19.12%.

3.3.3 Crystallography

Five expected complexes **I-V** are obtained and have been crystallographically characterized to be a dinuclear copper(II) complexes containing formato bridged while **VI** was characterized spectroscopically because the crystals of this complex were not of good enough quality to carry out a single-crystal X-ray diffraction structure determination.

Reflection data of **I-V** complexes were collected on a 4K Bruker SMART APEX CCD area-detector diffractometer with graphite monochromated Mo Kα radiation (λ= 0.71073 Å) (at a detector distance of 6.0 cm and swing angle of -28°) using SMART program. Raw data frame integration was performed with SAINT, which also applied correction for Lorentz and polarization effects. An empirical absorption correction by using the SADABS program was applied, which resulted in transmission coefficients ranging from 0.654 to 1.000, 0.8520 to 1.000, 0.7123 to 1.000, 0.773 to 1.000 and 0.7891 to 1.000 for **I-V**, respectively. The structure was solved by direct methods and refined by full–matrix least–squares method on $(F_{obs})^2$ with anisotropic thermal parameters for all non–hydrogen atoms except disordered O atoms of the ClO_4^- group and disordered F atoms of the PF_6^- groups using the SHELXTL-PC V 6.12 software package. The O atoms of the ClO_4^- group of **I** and **II** showed disorder; the occupancies of the disordered positions were initially refined and later fixed at 0.45 and 0.55 for **I** and 0.50 and 0.50 for **II**. The O atoms of the ClO_4^- group of **IV** also showed disorder. Attempts to model disordered positions into two sets are unsuccessful. However, their thermal parameters are substantially reasonable. For the structure determination of **III** and **V**, the two F atoms of each PF_6^- group showed disorder; the occupancies of the disordered positions were initially refined and later fixed at 0.47 and 0.53 for **III** and 0.49 and 0.51 for **V**. Furthermore, for **III**, one O atom of a formato group is also disordered and refined with site occupancies of 0.5. All hydrogen atoms of the dpyam ligands in **I** and **III** including one of formato ligand in **I** were geometrically fixed and allowed to ride on the attached atoms. Those of the bridging hydroxo and bridging methoxo groups in **I**, the bridging hydroxo and two bridging formato groups in **III** were located geometrically. All hydrogen atoms in **II**, **IV** and **V** were located geometrically and refined isotropically. The crystal and refinement details for complexes **I-V** are listed in Appendix IIIA.

3.4 Results and Discussion

3.4.1 Description of the crystal structures

3.4.1.1 Description of $[Cu_2(dpyam)_2(\mu\text{-}O_2CH)(\mu\text{-}OH)(\mu\text{-}OCH_3)](ClO_4)$ (I)

Complex **I** is a dinuclear unit copper(II) complex bridging by three different ligands. The structure of **I** consists of symmetric dinuclear $[Cu_2(dpyam)_2(\mu\text{-}O_2CH)(\mu\text{-}OH)(\mu\text{-}OCH_3)]^+$ cations with a single ClO_4^- counteranion. This unit is depicted in Fig. 2 together with the numbering scheme. Selected bond distances and angles are listed in Appendix IIIB.

Each copper(II) ion involves a CuN_2O_3 chromophore. The coordination geometry around each copper(II) ion is distorted trigonal bipyramidal ($\tau = 0.61$). The structure index is defined as $\tau = (\beta\text{-}\alpha)/60$, where β and α are the largest coordination angles[15]. The three longer bonds in the trigonal planar plane are a nitrogen atom of the dpyam ligand (Cu-N(2) distance 2.010(4) Å), an oxygen atom of the bridging formato ligand (Cu-O(3) distance 2.175(3) Å) and an oxygen atom of the bridging methoxo ligand (Cu-O(2) distance 2.169(5) Å). The two shorter bonds in the axial positions involve the other nitrogen atom of the dpyam ligand (Cu-N(1) distance 1.961(4) Å) and an oxygen atom of the bridging hydroxo ligand (Cu-O(1) distance 1.918(4) Å). This is typical for the trigonal bipyramidal geometry. The formate anion bridges two copper atoms in a syn-syn arrangement. The Cu-Cu distance is 3.023(1) Å. The bridging Cu(1)-O(1)-Cu(1A) and Cu(1)-O(2)-Cu(1A) angles are 104.0(3) and 88.3(2)°, respectively. The dpyam ligands are essentially planar, with only a dihedral angle of 6.9° between the individual pyridine rings. The bite angles of the dpyam ligands (N-Cu-N, 91.4 (2)°) are only slightly greater than 90°.

The lattice is further stabilized by hydrogen bonding between the amine N and the oxygen atom of bridging formato group with a N···O contact of 2.869 Å.

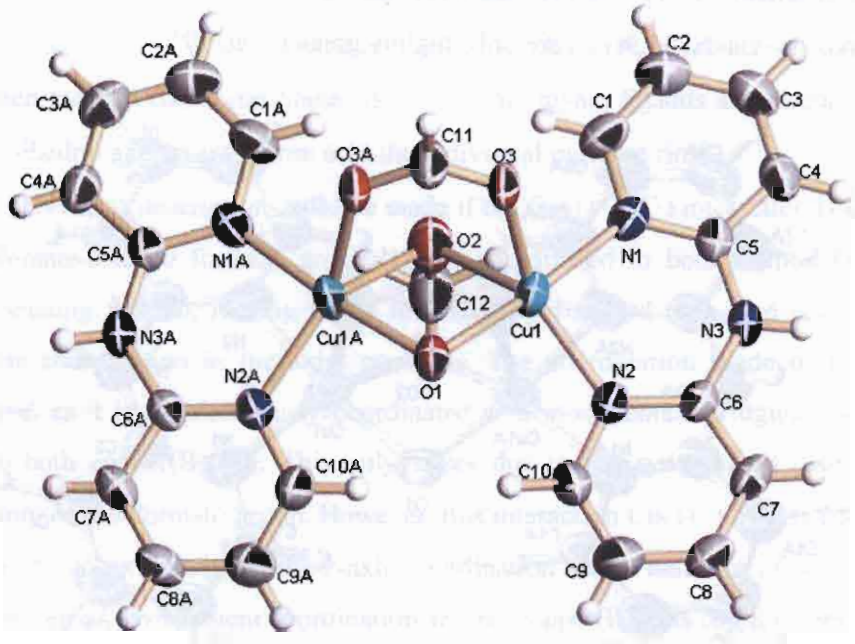

Figure 2 The molecular structure of **I**

3.4.1.2 Description of $[Cu_2(dpyam)_2(\mu\text{-}O_2CH)(\mu\text{-}OH)_2](ClO_4)\cdot H_2O$ (II)

The structure of **II** consists of a symmetric dinuclear $[Cu_2(dpyam)_2(\mu\text{-}O_2CH)(\mu\text{-}OH)_2]^+$ cation, with ClO_4^- counter anions. This unit is depicted in Fig. 3, together with the numbering scheme. Selected bond distances and angles are listed in Appendix IIIB.

Both copper(II) ions of the complex cation are linked through double hydroxo and a formato bridges, leading to a Cu–Cu distance of 2.902(1) Å. The coordination environment around each copper(II) ion can be best described as tetrahedrally distorted square pyramidal CuN_2O_2O' chromophore with a τ value of 0.27. The four shorter bonds in the basal plane involve two nitrogen atoms of the dpyam ligand (Cu-N 2.005(3) and 2.030(3) Å), two oxygen atoms of bridging hydroxo ligands (Cu-O 1.952(3) and 1.955 Å). An oxygen atom of the triatomic bridging formato ligand completes five-coordination at Cu(1) atom (Cu-O(3) 2.345 (3) Å), consistent with the typical square pyramidal geometry. The four basal atoms are not coplanar, showing a significant tetrahedral distortion with a dihedral angle of 23.8° formed between CuO_2 and CuN_2 planes and the copper atom is displaced by 0.189 Å from the basal plane toward the O(3) atom. The dinuclear unit is slightly planar and the dihedral angle between the basal N_2O_2 planes is 14.4°. The bridging Cu(1)-O(1)-Cu(1A) and Cu(1)-O(2)-Cu (1A) are 95.8(1) and 96.0(1)°, respectively. The dpyam ligands are essentially planar with

small dihedral angles of 6.6° between the individual pyridine rings. The bite angles of the dpyam ligands (N–Cu–N, 91.9(1)°) are only slightly greater than 90°.

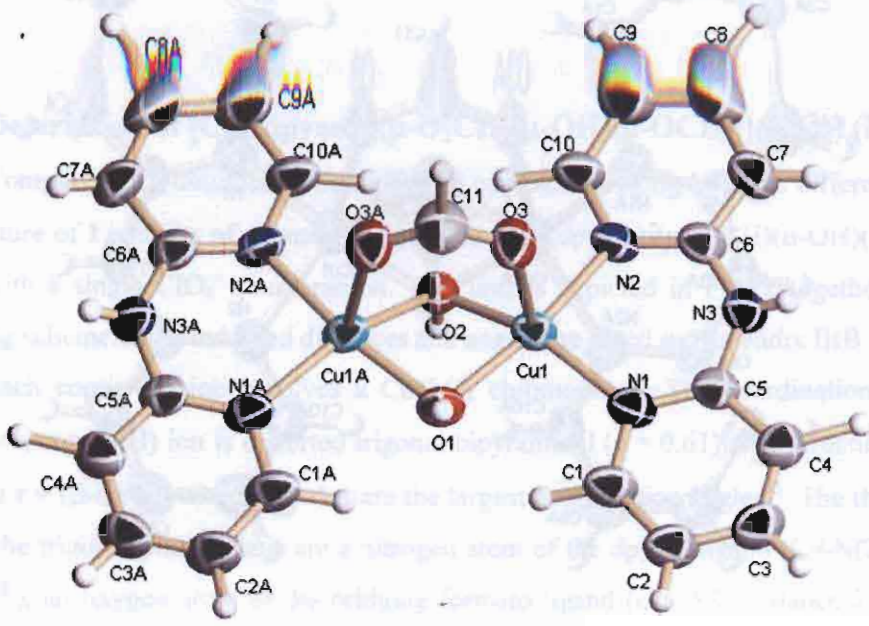

Figure 3 The molecular structure of **II**

3.4.1.3 Description of $[Cu_2(dpyam)_2(\mu\text{-}O_2CH)(\mu\text{-}OOCH)(\mu\text{-}OH)](PF_6)$ (III)

Complex **III** is made up of one-half $[Cu(dpyam)(\mu\text{-}O_2CH)_2(\mu\text{-}OH)]^+$ moiety, which the other half being inversion related and a disordered PF_6^- anion. This unit is depicted in Fig. 4 together with the numbering scheme. Selected bond distances and angles are listed in Appendix IIIB.

The formato ligands, which one of them is in a disordered position, in **III** exhibit different coordination mode. Both copper(II) ions within the dinuclear unit are bridged by three ligands, i.e. a hydroxo group and two formato ligands, which one formato ligand is in a familiar didentate syn,syn η^1: η^1: μ_2-bridging mode and the other is in the monoatomic bridging mode. A terminal dpyam ligand completes five coordination at each copper atom, which has a distorted trigonal bipyramidal geometry (τ = 0.59) of the CuN_2O_3 chromophore. An oxygen atom of the monoatomic bridged formato ligand (Cu(1)-O(2) 2.144(6) Å), an oxygen atom of the η^1: η^1: μ_2-bridging formato ligand (Cu(1)-O(4) 2.200(3) Å) and a nitrogen atom of the dpyam ligand (Cu(1)-N(2) 2.029(4) Å) comprise the trigonal plane. These equatorial distances are considerably longer than the two axial bonds occupied by an oxygen atom of the bridging hydroxo ligand (Cu(1)-O(1) 1.934(5) Å) and another nitrogen atom of the dpyam ligand (Cu(1)-N(1) 1.972(4) Å) corresponding to the typical environment of the

trigonal bipyramidal geometry. The Cu···Cu separation is 3.113(5) Å. The bridging Cu(1)-O (1)-Cu(1A), Cu(1)-O(2)-Cu(1A) angles are 107.2(4), 93.1(4)°, respectively. The dihedral angle between the two equatorial planes is 90.3°. The dpyam ligands are essentially planar, with only a dihedral angle varies from 6.1° the individual pyridine rings.

An alternative description could be made if the Cu(1)···O(3) interaction is considered. The monodentate-bridged formato group is also coordinated to both copper(II) ions in a didentate chelating fashion, leading to the tetrahedrally-distorted elongated octahedral with off-the-z-axis coordination in the axial positions. The coordination mode of this formato group is novel as it is simultaneously coordinated as a monodentate bridging and didentate chelating to both copper(II) ion. This only arises due to the symmetrical disorder of the second O atom of this formato group. However, this interaction Cu(1)···O(3) is considered to be weak due to an extremely-off-the-z-axis coordination and a half site of the O(3) atom. Hence, the preferred environment coordination around copper(II) ions could be best described as a distorted trigonal bipyramidal geometry.

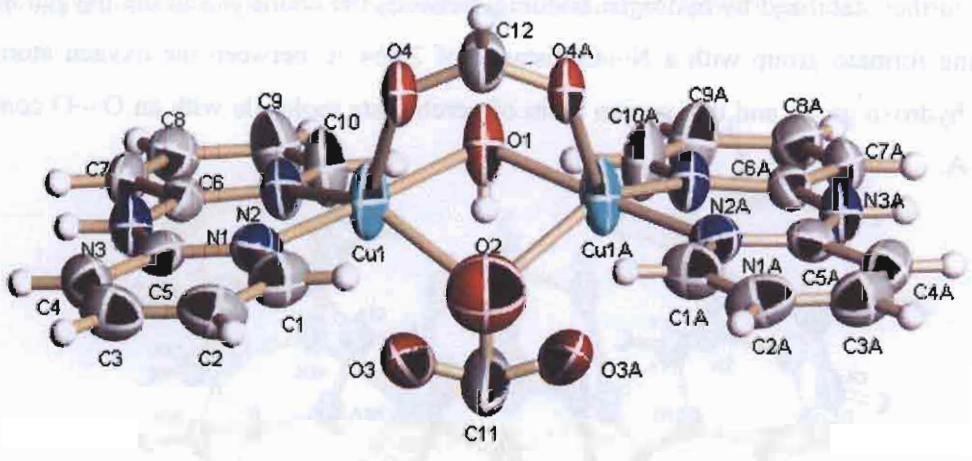

Figure 4 The molecular structure of **III**

The lattice is further stabilized by hydrogen bonding: between the amine N and the oxygen atom of bridging formato group with a N···O contact of 2.917 Å, between the carbon atom of dpyam ligand and the fluoride atom of PF_6^- anion with C···F distance of 3.099 Å.

3.4.1.4 Description of $[Cu_2(dpyam)_2(\mu\text{-}O_2CH)(\mu\text{-}OH)(\mu\text{-}Cl)](ClO_4)\cdot 0.5H_2O$ (IV)

The structure of **IV** consists of symmetric dinuclear $[Cu_2(dpyam)_2(\mu\text{-}O_2CH)(\mu\text{-}OH)(\mu\text{-}Cl)]^+$ cation, a ClO_4^- counter anion and half a molecule of lattice water. This unit is depicted in Fig. 5 together with the used numbering scheme. Selected bond distances and angles are listed in Appendix IIIB.

In the dinuclear unit the copper(II) ions are triply bridged through three different ligands, i.e. formate, chloride and hydroxide anions. Each copper(II) center is coordinated by two oxygen atoms and an chloride atom of the triple bridges and two nitrogen atoms of a dpyam ligand, leading to the five–coordinated, distorted trigonal bipyramidal geometry with CuN_2O_2Cl chromophore (τ = 0.60). The trigonal plane consists of a nitrogen atom of the dpyam ligand (Cu–N(2) distance 2.027(2) Å), a bridging chloro ligand (Cu–Cl(1) distance 2.478(2) Å) and an oxygen atom of the bridging formato ligand (Cu–O(2) distance 2.158(1) Å). The apical coordination sites are occupied by another nitrogen atom of the dpyam ligand (Cu–N(1) distance 1.975(1) Å) and an oxygen atom of the bridging hydroxo group (Cu–O(1) distance 1.916(1) Å). The Cu-Cu distance is 3.036(1) Å. The bridging Cu(1)-O(1)-Cu(1A) and Cu(1)-Cl(1)-Cu(1A) angles are 104.8(1) and 75.6(1)°, respectively. The dpyam ligands are planar, the dihedral angle between the individual pyridine rings is as low as 6.6°. The lattice is further stabilized by hydrogen bonding: between the amine N and the oxygen atom of bridging formato group with a N····O distance of 2.864 Å, between the oxygen atom of bridging hydroxo group and the oxygen atom of perchlorate molecule with an O····O contact of 2.922 Å.

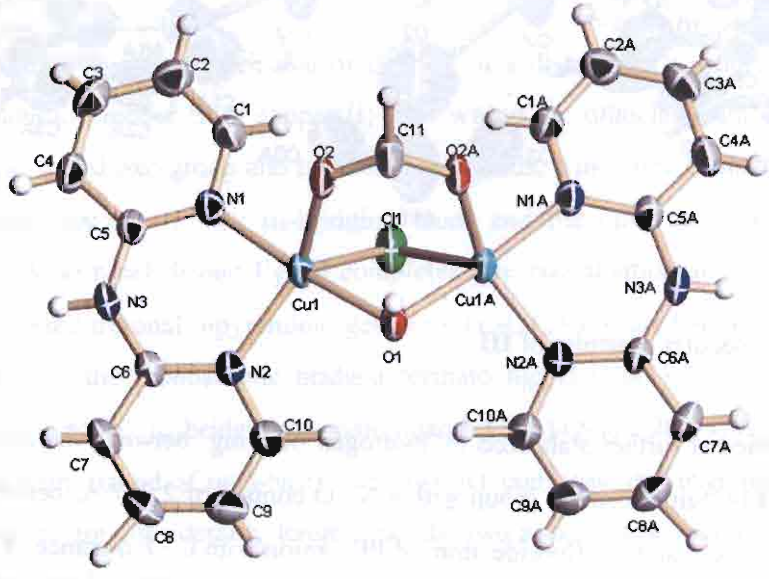

Figure 5 The molecular structure of **IV**

3.4.1.5 Description of $[Cu_2(dpyam)_2(\mu\text{-}O_2CH)(\mu\text{-}OH)(\mu\text{-}Cl)](PF_6)$ (V)

The structure of compound **V** is made up of a centrosymmetric dinuclear $[Cu_2(dpyam)_2(\mu\text{-}O_2CH)(\mu\text{-}OH)(\mu\text{-}Cl)]^+$ cation and a disordered PF_6^- counteranion. This unit is depicted in Fig. 6 together with the numbering scheme. Selected bond distances and angles are listed in Appendix IIIB.

Each copper(II) ion has a distorted trigonal bipyramidal geometry (τ = 0.72, the structure index is defined as $\tau = (\beta\text{-}\alpha)/60$, where β and α are the largest coordination angles), of the CuN_2O_2Cl chromophore, with a nitrogen atom of the dpyam ligand (Cu(1)-N(1) 2.031 (3) Å), an oxygen atom of the bridging formato ligand (Cu(1)-O(1) 2.183(2) Å) and a bridging chloro ligand (Cu(1)-Cl(1) 2.451(1) Å) forming the trigonal plane. The axial site of each copper(II) atom is occupied by another nitrogen atom of the dpyam ligand (Cu(1)-N(2) 1.983(2) Å) and an oxygen atom of the hydroxo ligand (Cu(1)-O(2) 1.918(2) Å, which are shorter than those of the equatorial plane corresponding to the typical environment of the trigonal bipyramidal geometry. The symmetric syn, syn-coordinated formato ligand bridges the two equatorial planes, leading to a Cu···Cu distance of 3.061(5) Å. The dihedral angle between the equatorial planes is 86.8°. The bridging angles (Cu(1)-O(2)-Cu(1A) and Cu(1)-Cl (1)-Cu(1A) are 105.9(1) and 77.2(1)°, respectively. The dpyam ligands are essentially planar, with only a dihedral angle of 4.4° between the individual pyridine rings.

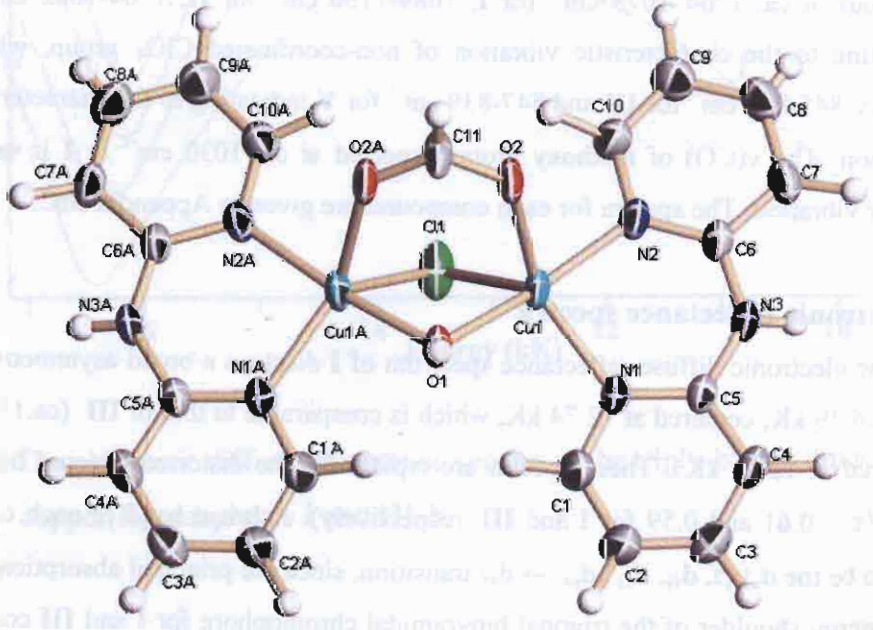

Figure 6 The molecular structure of **V**

The lattice is further stabilized by hydrogen bonding: between the amine N and the oxygen atom of bridging formato group with a N···O distance 2.857 Å, between the oxygen atom of bridging hydroxo group and the fluoride atom of PF_6^- anion with O···F contact of 2.961 Å.

3.4.2 IR spectra

The infrared spectra display a broad band at 3467, 3500, 3580, 3449 and 3563 cm^{-1} for **I-V**, respectively, which can be assigned to the bridging OH vibrations of the hydroxo bridged. The spectra also exhibit the broad and intense bands at 1570 cm^{-1} for **I** and **IV**, 1571 cm^{-1} for **II** and **V** corresponding to the $\nu_{as}(COO^-)$ vibration and a medium broad band at 1344 cm^{-1} for I, 1350 cm^{-1} for **II**, 1357 cm^{-1} for **IV** and 1354 cm^{-1} for **V** corresponding to the ν_s (COO^-) vibration, the difference Δ [$\Delta = \nu_{as}(COO^-) - \nu_s(COO^-)$; 226 cm^{-1} for **I**, 220 cm^{-1} for **II**, 213 cm^{-1} for **IV** and 217 cm^{-1} for **V**] is close to that of NaO_2CH (201 cm^{-1}) as expected for the triatomic bridging coordination mode of the formate group within a dinuclear species. Due to the formato bridges in **III** are present in different coordination modes, two $\nu_{as}(COO^-)$ 1603, 1586 cm^{-1} and two ν_s (COO^-) 1411, 1346 cm^{-1} bands are observed in the IR spectrum. The bands at 1603, 1346 cm^{-1} (Δ = 257 cm^{-1}) are assigned to the stretching modes of the monoatomic formato bridges. The vibrations observed at 1586, 1411 cm^{-1} (Δ = 175 cm^{-1}) are consistent with the triatomic carboxylato bridge. Moreover, the spectra exhibit the broad and intense bands at ca. 1104–1078 cm^{-1} for **I**, 1089-1100 cm^{-1} for **II**, 1104-1082 cm^{-1} for **IV** corresponding to the characteristic vibration of non-coordinated ClO_4^- group, while those appear at ca. 845-840 cm^{-1} for **III** and 847-839 cm^{-1} for **V** indicating to the characteristic band of PF_6^- anion. The ν(CO) of methoxy group expected at ca. 1030 cm^{-1} in **I** is masked by perchlorate vibration. The spectra for each compound are given in Appendix IIIC.

3.4.3 Electronic reflectance spectra

The electronic diffuse reflectance spectrum of **I** displays a broad asymmetric band at ca. 12.20-14.49 kK, centered at 12.74 kK, which is comparable to that of **III** (ca.11.49-14.60 kK, centered at 12.81 kK). These spectra are typical for the distorted trigonal bipyramidal geometry (τ = 0.61 and 0.59 for **I** and **III**, respectively). A broad band of each complex is assigned to be the d_{x2-y2}, d_{xy}, d_{xz}, $d_{yz} \rightarrow d_{z2}$ transition, since the principal absorption peak and a higher energy shoulder of the trigonal bipyramidal chromophore for **I** and **III** could not be resolved. A regular trigonal bipyramidal geometry is usually characterized by an asymmetric broad peak at ca. 11.50 kK with a possible high-energy shoulder at ca. 14.50 kK. The

principal absorption may be assigned as a $d_{x2-y2} \rightarrow d_{z2}$ transition, with the high-energy shoulder assigned as a $d_{xz} \approx d_{yz} \rightarrow d_{z2}$. The spectra of **IV** and **V** show broad asymmetric peaks at approximately 11.96 and 11.98 kK, respectively, with some evidences for a possible high-energy shoulders at ca. 14.29 and ca. 14.30 kK consistent with the distorted trigonal bipyramidal geometry (τ = 0.60 for **IV** and 0.72 for **V**). The principal absorption may be assigned as a $d_{x2-y2} \rightarrow d_{z2}$ transition, with the high-energy shoulder assigned as a $d_{xz} \approx d_{yz} \rightarrow d_{z2}$.

The electronic diffuse reflectance spectrum of **II** show a broad band centered at 13.99 kK. This observed single broad peak is consistent with the tetrahedrally-distorted square pyramidal stereochemistry[4-10] and assigned to be the d_{z2}, d_{xy}, d_{xz}, d_{yz}, $\rightarrow d_{x2-y2}$ transition.

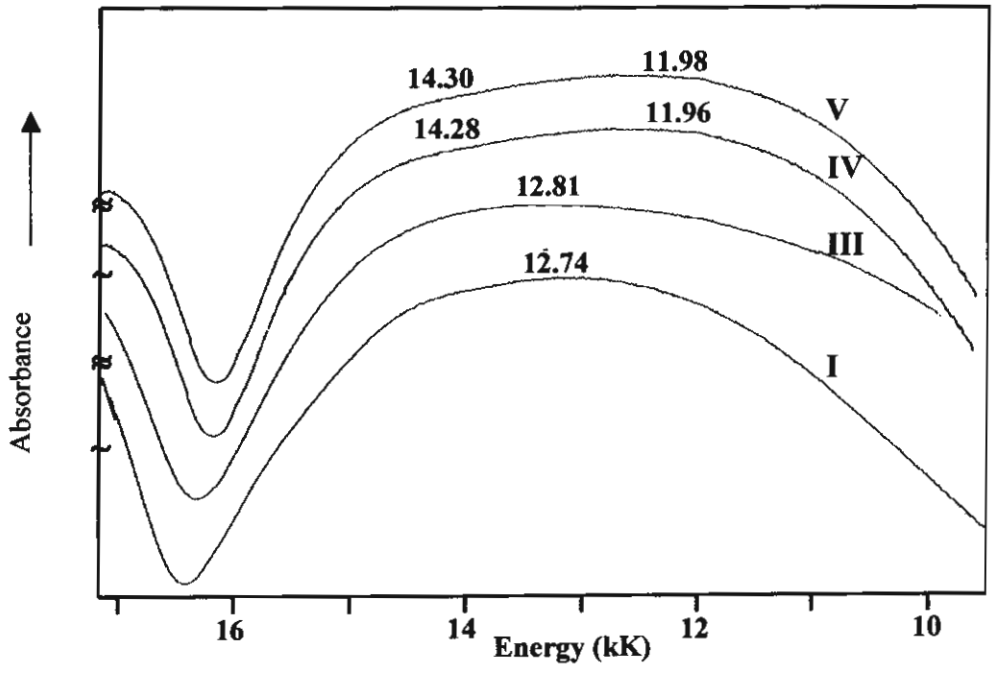

Figure 7 The electronic diffuse reflectance spectra of the triply-bridge dinuclear copper(II) complexes **I** and **III-V**

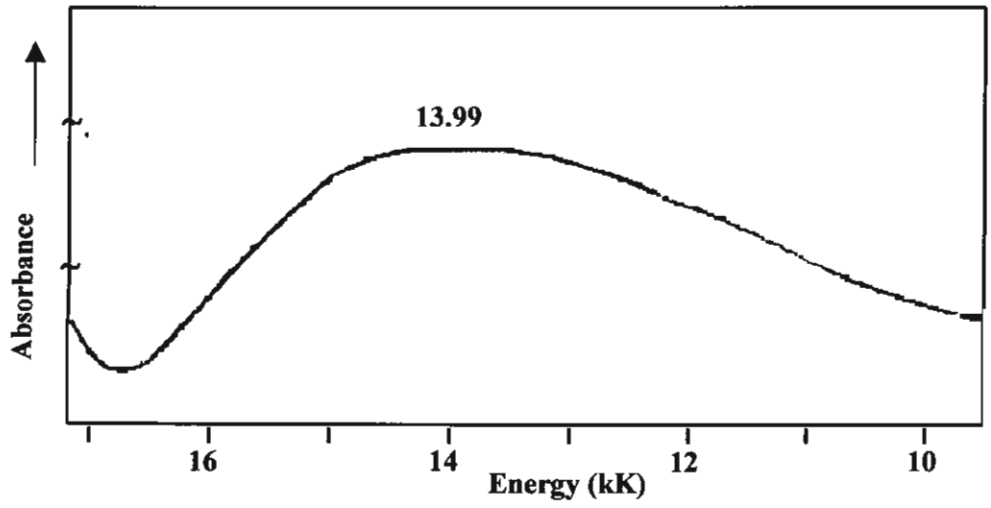

Figure 8 The electronic diffuse reflectance spectra of the triply-bridge dinuclear copper(II) complexes $[Cu_2(dpyam)_2(\mu\text{-}O_2CH)(\mu\text{-}OH)_2](ClO_4)\cdot H_2O$ **(II)**

3.4.4 EPR spectra

The X-band polycrystalline EPR spectra of $[Cu_2(dpyam)_2(\mu\text{-}O_2CH)(\mu\text{-}OH)(\mu\text{-}OCH_3)](ClO_4)$ **(I)** (Appendix IIID) at room temperature and liquid nitrogen temperature (77 K) are either very weak and display an isotropic copper(II) signal at 2.10 and 2.10, respectively, while a triplet state signal at g ≈6.96 (≈160 mT) are not observed properly. The former feature is most certainly from a monomeric Cu(II) impurity, which is always present in dinuclear species. The isotropic-typed EPR of the almost compounds spectra give no information regarding to the ground state, due to the misalignment of the CuN_2O_3 chromophore. A triplet state signal usually attributed to intramolecular exchange interaction between two unpair electrons of copper atoms, $\Delta M_s = \pm 2$ transition. The room temperature and 77 K EPR spectra of complexes $[Cu_2(dpyam)_2(\mu\text{-}O_2CH)(\mu\text{-}OOCH)(\mu\text{-}OH)](PF_6)$ **(III)**, $[Cu_2(dpyam)_2(\mu\text{-}O_2CH)(\mu\text{-}OH)(\mu\text{-}Cl)](ClO_4)\cdot 0.5H_2O$ **(IV)** and $[Cu_2(dpyam)_2(\mu\text{-}O_2CH)(\mu\text{-}OH)(\mu\text{-}Cl)](PF_6)$ **(V)** also indicated isotropic signal, while those of $[Cu_2(dpyam)_2(\mu\text{-}O_2CH)(\mu\text{-}OH)_2](ClO_4)\cdot H_2O$ **(II)** is silent. The spectra for each compound are given in Appendix IIID.

3.4.5 Magnetic properties and superexchange mechanism

The effective magnetic moment (μ_{eff}) measuring by the Faraday method at room temperature are 2.50, 2.54, 2.50 and 2.53 μ_B for **I**, **III**, **IV** and **V**, respectively, which is close to the normal value (2.45 μ_B) of the uncoupled d^9 copper(II) ions suggesting noninteraction between the copper(II) centers in dimeric complexes at room temperature.

The magnetic properties of compounds **I** and **IV** mutually show a very similar behaviour and are depicted in in the form of μ_{eff} *versus* T for two copper(II) ions (Figs. 9 and 10 respectively), also in the form of μ_{eff} versus T for two Cu(II) ions. At 280 K, μ_{eff} is 2.561 μ_B for compound **I** (2.781 μ_B for compound **IV**) which agrees well with the spin-only value of Cu(II) calculated for two uncoupled spin =1/2 centres. Upon cooling, it raises gradually to reach 2.741 μ_B and 2.97 at 30 K, for compounds **I** and **IV**, respectively. This is typical for a ferromagnetically coupled Cu(II) dinuclear compound. Below that temperature, μ_{eff} then diminishes till a value of 2.631 μ_B at 5 K for compound **I** (2.76 for compound **IV**), which may originate from intermolecular antiferromagnetic interactions, or from zero-field splitting of the S = 1 state of the dinuclear species.

The theoretical expression for the magnetic susceptibility for two interacting S = 1/2 centres, which is based on the general Hamiltonian[16], is $H_{ex} = -JS_1S_2$, in which the exchange parameter J is negative for antiferromagnetic and positive for ferromagnetic interaction. The magnetic data were fitted to the equation given in the literature for dinuclear copper compounds

$$\chi_m = (2Ng^2\beta^2)[kT-(2\,zJ'/(3+\exp(-J/kT)))]^{-1}\,[3+\exp(-J/kT)]^{-1}\,(1-p)+\chi_m p + \text{TIP}$$

in which N, g, β, k and T have their usual meanings. The parameter p denotes the fraction of paramagnetic impurity in the sample and zJ' the interaction between neighboring dinuclear identities. A temperature independent paramagnetism (TIP) was also considered and fixed at 60 x 10^{-6} per copper ion. The best fit was obtained with the following values: J = 62.5 cm^{-1}, g = 1.99, zJ' = -3.80 cm^{-1}, p = 0.06, with a final R of 1.4 x 10^{-3} (Fig. 9). For compound **IV**, these values are J = 79.1 cm^{-1}, g = 2.14, zJ' = -4.27 cm^{-1}, p = 0.025, with a final R of 1.6 x 10^{-3} (Fig. 10).

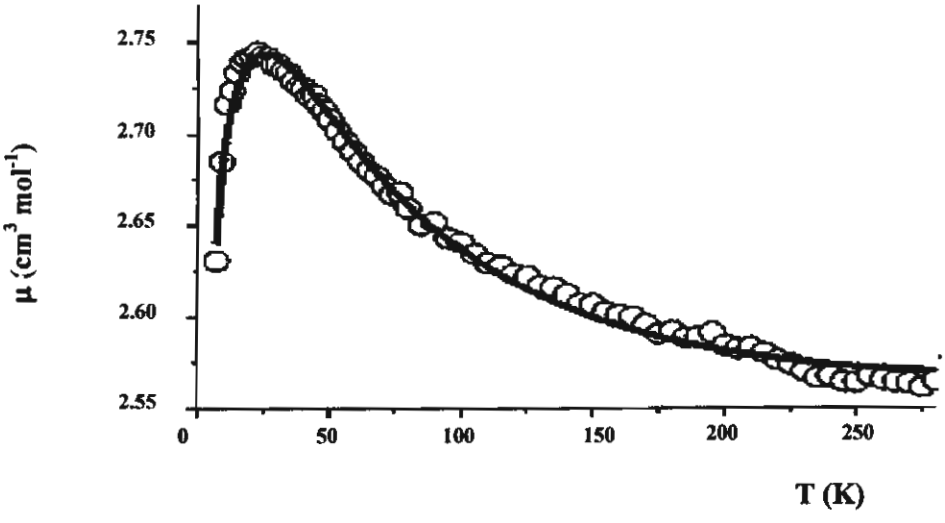

Figure 9 A plot of the temperature dependence of μ_{eff} *vs.* T for compound **I**

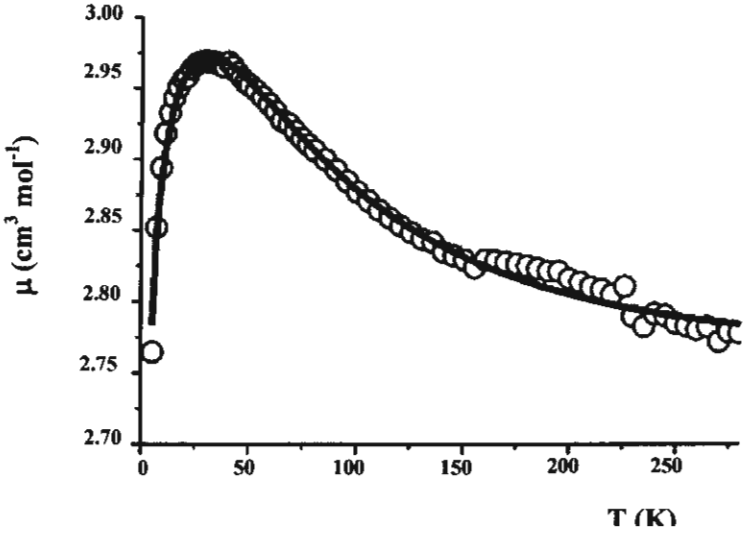

Figure 10 A plot of the temperature dependence of μ_{eff} *vs.* T for compound **IV**

The magnetic properties compounds **III** and **V** mutually show a very similar behaviour. At 280 K μ_{eff} is 2.45 μ_B for compound **III** (2.45 μ_B, for **V**) which agrees reasonable with the spin-only value of Cu(II) calculated for two uncoupled spin = ½ centres. Upon cooling it raises gradually to reach 2.59 and 2.60 at around 30 K, for compounds **III** and **V**, respectively. This is typical for a ferromagnetically coupled Cu(II) dinuclear compound. Below that temperature, μ_{eff} then diminishes till a value around 2.45 μ_B at 5 K for compounds **III** and **V**, which may originate from intermolecular antiferromagnetic interactions, or from zero-field splitting of the S = 1 state of the dinuclear species.

The theoretical expression for the magnetic susceptibility for two interacting S = 1/2 centres, which is based on the general Hamiltonian is: $H_{ex} = -JS_1S_2$, in which the exchange parameter J, is negative for antiferromagnetic and positive for ferromagnetic interaction. The magnetic data were fitted to the equation given in the literature for dinuclear copper compounds

$$\chi_m = (2Ng^2\beta^2)[kT-(2\,zJ'/(3 + \exp(-J/kT)))]^{-1}\,[3 + \exp(-J/kT)]^{-1}\,(1-p) + \chi_M p + \text{TIP}$$

in which N, g, β, k and T have their usual meanings. The parameter p denotes the fraction of paramagnetic impurity in the sample and zJ' the interaction between neighbouring dinuclear identities. A temperature independent paramagnetism (TIP) was also considered and fixed at 60 x 10^{-6} per copper ion.

The best fit was obtained for compound **III** with the following values: J = 30.8 cm^{-1}, g = 1.95, zJ'= -8.29 cm^{-1}, p = 0.00, with a final R of 3.0 x 10^{-3} (Fig. 11). For compound **V**

these values are J = 36.7 cm^{-1}, g = 1.95, zJ'= -6.32 cm^{-1}, p = 0.06, with a final R of 5.7 x 10^{-3} (Fig. 12).

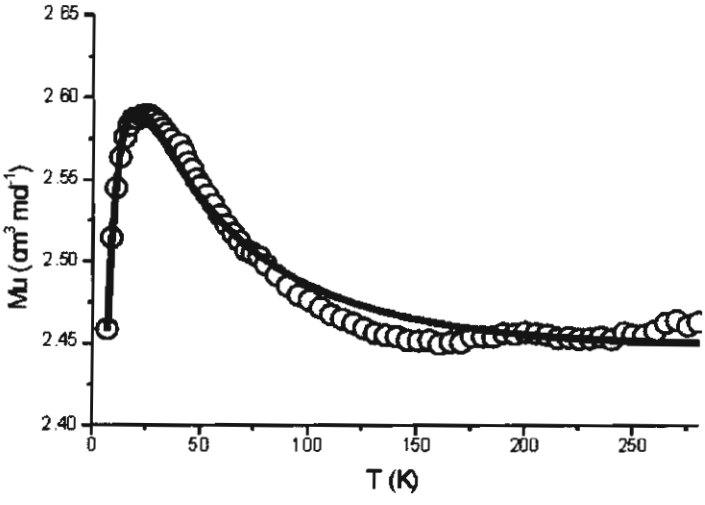

Figure 11 A plot of the temperature dependence of μ_{eff} *vs.* T for compound **III**

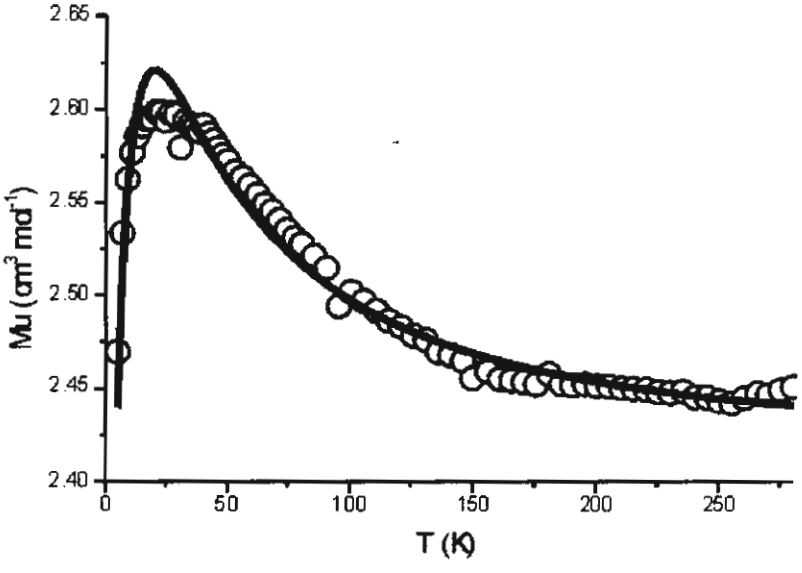

Figure 12 A plot of the temperature dependence of μ_{eff} *vs.* T for compound **V**

The obvious explanation for the triply-bridged dinuclear copper(II) complexes lies in the fact that the most complexes have a distorted square pyramidal stereochemistry with d_{x2-y2} ground states. A hydroxo ligand bridges from an equatorial position at one copper(II) ion to an equatorial positions at the other and contribute the antiferromagnetic interaction, which is

the general trend for increased antiferromagnetic coupling with increasing hydroxide bridge angle. The considerably reduced antiferromagnetic contribution is attributed to the reduced σ overlap between the oxygen p orbital and the copper(II) $d_{x^2-y^2}$ orbital. This relation would be expected for the intermediate geometry with possibly some mixture of the d_{z^2} character in the axial position that reduce electron density in the $d_{x^2-y^2}$ orbital. A change in electron density of the magnetic orbital can have a pronounced effect on the sign and magnitude of a magnetic exchange interaction.

The coordination geometry around each copper(II) ion of **I**, **III**, **IV** and **V** is distorted trigonal bipyramidal, which the unpaired electron resides primarily in d_{z^2} orbital with orientation along the apical hydroxo bridging ligand. In this case a major σ pathway via (Cu-OH-Cu) is possible for the electron delocalization via the d_{z^2} magnetic orbitals, corresponding to the weak or strong ferromagnetic interaction (Fig. 13). The unpair electron of first copper ion couple with an electron in p-orbital of oxygen atom and the unpair electron of second copper ion couple with an electron in other p-orbital of oxygen atom resulting to two unpair electrons in p-orbital. A strong magnetic interaction requires both good σ orientation of the magnetic orbitals and good superexchange properties of the bridging atom(s). Therefore this case indicates a moderate ferromagnetic exchange.

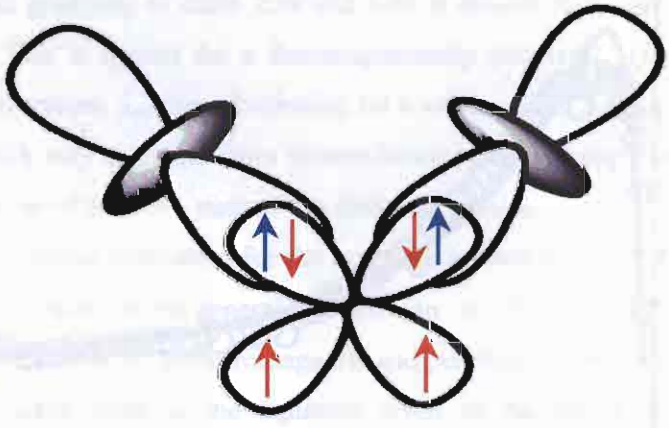

Figure 13 The proposed superexchange mechanism in **I** through oxygen p-orbitals of hydroxo bridging ligand

It should be noted that when the copper(II) geometry is close to regular square pyramidal, an often strong antiferromagnetic interaction will be predominant, but a reduction of an antiferromagnetic contribution will be observed when the geometry becomes closer to trigonal bipyramidal (Table 1).

The complex $[Cu_2(dpyam)_2(\mu\text{-}O_2CH)(\mu\text{-}OH)_2](ClO_4)\cdot H_2O$ **(II)** exhibits a distorted square pyramidal geometry, which the unpaired electron is located in a $d_{x^2-y^2}$ type orbital. The

$d_{x^2-y^2}$ magnetic orbital in **II** is directed toward the dihydroxo-bridged, the Cu-O-Cu angles of 95.8 and 96.0°. For these bridging angles, a moderate antiferromagnetic coupling (J = -122.54 cm^{-1}) should be expected following Hodgson and Hatfield's linear relationship[17] which is usually applied successfully for the planar dihydroxo bridge complexes (Fig. 14).

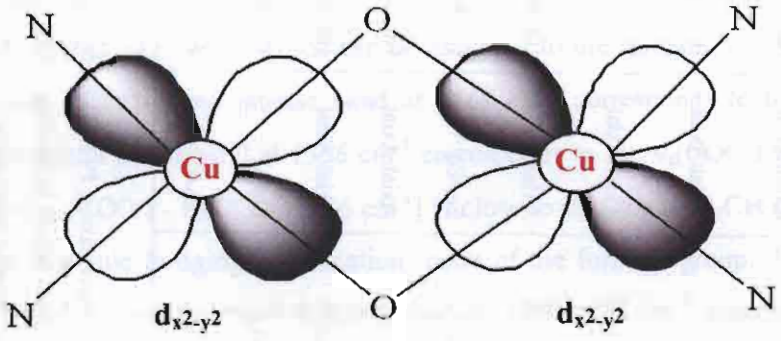

Figure 14 The proposed superexchange mechanism in **II** through oxygen p-orbitals of hydroxo bridges